Sediment archives reveal irreversible shifts in plankton communities after World War II and agricultural pollution

Raffaele Siano, Malwenn Lassudrie, Pierre Cuzin, Nicolas Briant, Véronique Loizeau, Sabine Schmidt, Axel Ehrhold, Kenneth Neil Mertens, Clément Lambert, Laure Quintric, et al.

Current Biology
June 2021, Volume 31 Issue 12 Pages 2682-2689.e7
https://doi.org/10.1016/j.cub.2021.03.079
https://archimer.ifremer.fr/doc/00690/80195/

Sediment archives reveal irreversible shifts in plankton communities after World War II and agricultural pollution

Siano Raffaele [1, *], Lassudrie Duchesne Malwenn [2], Cuzin Pierre [3], Briant Nicolas [4], Loizeau Veronique [5], Schmidt Sabine [6], Ehrhold Axel [7], Mertens Kenneth [2], Lambert Clément [8], Quintric Laure [3], Noël Cyril [3], Latimier Marie [1], Quéré Julien [1], Durand Patrick [3], Penaud Aurélie [9]

[1] Ifremer, DYNECO, 29280 Plouzané, France
[2] Ifremer, LITTORAL LER BO, Station de Biologie Marine, Place de la Croix, BP40537, 29900 Concarneau Cedex, France
[3] Ifremer, SeBiMER, 29280 Plouzané, France
[4] Ifremer, BE, 44311 Nantes, France
[5] Ifremer, PFOM, 29280 Plouzané, France
[6] CNRS, UMR 5805 EPOC, Université de Bordeaux, Pessac, France
[7] Ifremer, GM, 29280 Plouzané, France
[8] UMR 6538 Laboratoire Géosciences Océan (LGO), Université de Bretagne Sud (UBS), 56000 Vannes, France
[9] CNRS, UMR 6538 Laboratoire Géosciences Océan (LGO), Université de Brest (UBO), 29280 Plouzané, France

* Corresponding author : Raffaele Siano, email address : raffaele.siano@ifremer.fr

Abstract :

To evaluate the stability and resilience1 of coastal ecosystem communities to perturbations that occurred during the Anthropocene,2 pre-industrial biodiversity baselines inferred from paleoarchives are needed.3,4 The study of ancient DNA (aDNA) from sediments (sedaDNA)5 has provided valuable information about past dynamics of microbial species6, 7, 8 and communities9, 10, 11, 12, 13, 14, 15, 16, 17, 18 in relation to ecosystem variations. Shifts in planktonic protist communities might significantly affect marine ecosystems through cascading effects,19, 20, 21 and therefore the analysis of this compartment is essential for the assessment of ecosystem variations. Here, sediment cores collected from different sites of the Bay of Brest (northeast Atlantic, France) allowed ca. 1,400 years of retrospective analyses of the effects of human pollution on marine protists. Comparison of sedaDNA extractions and metabarcoding analyses with different barcode regions (V4 and V7 18S rDNA) revealed that protist assemblages in ancient sediments are mainly composed of species known to produce resting stages. Heavy-metal pollution traces in sediments were ascribed to the World War II period and coincided with community shifts within dinoflagellates and stramenopiles. After the war and especially from the 1980s to 1990s, protist genera shifts followed chronic contaminations of agricultural origin. Community composition reconstruction over time showed that there was no recovery to a Middle Ages baseline composition. This demonstrates the irreversibility of the observed shifts after the cumulative effect of war and agricultural pollutions. Developing a paleoecological approach, this study highlights how human contaminations

irreversibly affect marine microbial compartments, which contributes to the debate on coastal ecosystem preservation and restoration.

Results and Discussion

Paleocommunity diversity of marine coastal ecosystems

Biological analyses on microeukaryotic (protist) communities were inferred from sediment cores collected at three different sites of the Bay of Brest (Figure S1A) covering about 72 (Elorn Estuary core [EE] Data S1A), 99 (Daoulas Estuary core [DE] Data S1B) and 5000 calendar years (cal. yr.) (Brest Harbor core (BH], Figure S1B, Data S1C, Video S1). The multiple sedimentary ancient DNA (*sed*aDNA) extraction methods combined with a double metabarcoding analysis that were applied to the BH core provided new information for the future establishment of a general protocol for marine *sed*aDNA studies. After validation on the BH core, this approach was applied to EE and DE cores. By comparing total (TOT), intracellular (IN) and extracellular (EX) *sed*aDNA extraction methods (Table S1, Figure S2A, Figure S2B), and the α and β protist diversities obtained from two different barcode sizes (V4 [ca. 390 bp, base pairs] and V7 [ca. 200 bp] of the 18S ribosomal DNA [rDNA] gene region) (Table S2), it was found that the total *sed*aDNA extraction method allowed the analysis of mostly intracellular DNA (Figure S2C, Figure S2D). Over the entire BH core, up to 69% of V7 and 58% of V4 Amplicon Sequence Variants (ASVs) that were ≥ 1% abundant in the TOT extracts, were also present in the IN fraction (Figure S2E). Our study confirms Armbrecht et al.'s[22] hypothesis that extraction techniques targeting only extracellular DNA, as those used in terrestrial ecological surveys[23,24], are not suitable for marine *sed*aDNA studies of protists. Given the ability of many protists to form benthic, sedimentary resting stages that protect cellular content—including the nucleus—it is considered that the retrieved intracellular protist DNA is extracted from resting stages. Indeed, 83% (V7) and 82% (V4) of the common ASVs were assigned to protist genera known to include species that can produce resting stages (Data S2). It is suggested that the amplification of total *sed*aDNA allows diversity analyses of mostly protist resting stages and that eukaryotic DNA archives in ancient sediments mostly correspond to assemblages of protist resting stages, that are defined here as paleocommunities.

BH sediment samples could be separated into two groups according to ASV richness and β diversities (Figure S2D). This difference was attributed *sed*aDNA preservation issues in sandy

lower deposits of deeper core layers. Therefore, only the first upper section of the BH core (0-231 cm, ca. 1400 years from the Middle Ages [Vth–VIth centuries] to the contemporary era [XXIth century]) was considered for biodiversity analyses (Figure S2F). *Sed*aDNA metabarcoding analyses of the BH core showed that the long (V4) and the shorter (V7) fragments provided a similar diversity for eukaryotic paleocommunities (Figure 1). Although only some eukaryotic groups were identified by V7 metabarcoding (unknown Archaeplastida, Telonemia), V4 analysis allowed to identify more groups than V7 (33 vs 27). Therefore, only V4 was considered in the subsequent ecological analyses of the Bay of Brest cores. Degradation of *sed*aDNA involves DNA fragmentation[22], therefore the length of the barcode used in metabarcoding influences biodiversity analyses. The amplification of ca. 500 bp fragments from ancient sediment for some protist species was previously reported in ancient sediments (e.g.[10]). In agreement with previous results, here it is demonstrated that ca. 400 bp DNA fragment analyses are also suitable for assessing the diversity of a large fraction of the protist community, confirming that the previous validation of the V4 approach of Medieval (until ca. AD 900) to modern sediment from freshwater environments[13] also works for coastal marine ecosystems.

Paleocommunities of the BH core were mostly composed of three divisions: Alveolata, Opisthokonta, and Archaeplastida, dominated respectively by Apicomplexa (average: 33%), Metazoa (12%), and Streptophyta (8%). Dinoflagellata (Alveolata) (6%) were the fourth abundant group. Unassigned eukaryotic ASV (Unknown) accounted for on average 28% of the paleocommunity biodiversity (Figure 1, right panel). The relative importance of the most important groups varied throughout the core. Metazoa largely dominated in superficial sediments (3–11 cm; average: 45%, max: 70%) with Annelida ASV as the most representative phylum (average 38%). The protist group of Apicomplexa usually dominated throughout the rest of the BH core (13–231 cm; average: 30%; max: 59%; Figure 1) and the EE and DE cores (Figure S3). Within this group the invertebrate parasitic class of gregarines were prevalent (average: 25%; max: 55% of total

eukaryotes), dominated by three genera of invertebrate coelomic parasites[25] (average, max: *Lecudina*, 15%, 50%; *Lankesteria*, 2%, 8%; *Selenidium*, 1%, 8%). Dinoflagellates were occasionally abundant both in superficial (22%; 23%) and in deeper sediments (14%; 20%).

Paleocommunities differ from both superficial sediment and planktonic protist communities. In plankton communities, the supergroup of Alveolata (specifically Marine ALVeolates (MALVs) and dinoflagellates) dominate together with Rhizaria and Stramenopiles (particularly Bacillariophyta), respectively, the offshore[26] and the coastal protist communities[27]. Superficial sediment communities are dominated by Rhizaria (in particular Cercozoa), Alveolata (Ciliophora), and Stramenopiles (Bacillariophyta), and share < 10% of the species richness with the planktonic community[28]. The dominance or high proportion of gregarines, a resting-stage-forming group of metazoan parasites[29], can be considered a specific protist biodiversity pattern of marine sediment archives. Indeed, Apicomplexa were also found abundant in marine sedimentary archives of the Arabian Sea and associated to depleted oxygen conditions[15]. Gregarines in particular, were dominant in soil protist communities of Neotropical forests, findings that suggest those groups shape animal diversity in forest ecosystems[30]. Similarly, these parasites could contribute to shape marine animal communities in a marine ecosystem. Their dominance in centuries-old protist paleocommunities could suggest long-term parasitic pressure over animal communities. Hence, gregarines may have a trans-ecosystem functional role, and protist paleocommunities, in both soils and marine sediments, might reveal long-term host-parasite ecological patterns.

Paleocommunity shifts in relation to coastal pollution

The multivariate regression tree (MRT) analysis suggested that shifts in the protist communities occurred during the 1930s–40s and 1980s–90s (Figure S3). The protist groups largely responsible for these shifts were dinoflagellates (Figure 2) and stramenopiles (Figure 3).

123 Dinoflagellate communities drastically changed during the 1940s (break point 1941, BH
124 core) shifting from the dominance of suessioid genera (*Pelagodinium* and *Biecheleria*/*Protodinium*,
125 Figure 2) during the entire Middle Age and the XIXth century to the beginning of the XXth century
126 to a dominance of gonyaulacoid genera (*Gonyaulax* and *Alexandrium*, Figure 2) during the end of
127 the XXth and beginning of the XXIth centuries. Suessioid genera almost disappeared after the 1980s
128 (1987, DE), they are indeed relatively rare in current coastal plankton[27], and peridinioid genera
129 became more important (Figure 2). Changes in the relative importance of the genus *Gonyaulax*
130 largely explain dinoflagellate variations. The genus *Gonyaulax* progressively decreased in
131 importance after the 1980s (1987, DE) and the 1990s (1998, EE), whereas the genera *Heterocapsa*
132 (peridinioid) and the potentially harmful genus *Alexandrium* increased in importance (Figure 2).
133 This result confirms previous observations of increased abundance of the toxic species *Alexandrium*
134 *minutum* revealed by real-time PCR analyses on *sed*aDNA from the same DE and EE cores in
135 parallel with the recrudescence of harmful algal blooms caused by this species over the time in the
136 Bay of Brest[7].
137 Stramenopiles also drastically shifted during the 1940s and 1950s (Figure 3). The
138 heterotrophic group MAST (MArine STramenopiles[31]) and in particular the MAST-12 clade
139 dominated stramenopile paleocommunities during the Middle Age and the XIXth century (Figure
140 3). The relative abundance of Bacillariophyta (diatoms) started to increase during the XXth century
141 (1942, DE) and dominated after the 1950s (1952, BH) with MAST-12 progressively decreasing in
142 abundances (Figure 3). Within the diatom community, *Chaetoceros* was progressively replaced by
143 the genus *Thalassiosira* as well as by other unidentified diatoms after the 1990s (1998, EE) (Figure
144 3).
145 As noted, genera found in pre-war sediments became very rare after the World War II
146 (WWII) period and conversely current dominant genera were rare in the past. This indicates that

147 the community shifts observed in this study were irreversible at the time scale of our paleogenetic
148 analyses.

149 To infer potential causes of paleocommunity shifts in the Bay of Brest, contaminants were
150 analyzed in sediment samples of the BH core. Three groups of heavy metals were discriminated in
151 sediment samples (non-parametric correlation, Spearman test, $p < 0.05$; Figure 4, Figure S4A,
152 Figure S4B, Figure S4C) and concentrations of aluminum (Al)-normalized lithium (Li), nickel (Ni),
153 mercury (Hg), and lead ($^{206}Pb/^{207}Pb$) were examined in the sediment samples (Figure 4, Figure
154 S4D) as representative of each of the three groups. Li normalized concentrations and dynamics
155 were constant across the studied interval (12.9 ± 0.8 mg kg^{-1} (mean ± SD). Ni had constant
156 normalized concentrations throughout the core (4.8 ± 0.2 mg kg^{-1}) with the exception of two peaks
157 detected in the years 1947 ± 11 (WWII period) and 1913 ± 16 (WWI period) (concentration increase
158 of up to 50%, 9.8 mg kg^{-1}) (Figure 4). At 1936 ± 12 (WWII period), a small $^{206}Pb/^{207}Pb$ peak was
159 also detected. Hg increased its normalized concentrations from 1958 ± 9 to more recent times
160 (surface layers) with a peak at 1981 ± 5 (Figure 4). To evaluate whether pollutant sources were of
161 an anthropogenic origin, the relative enrichment factor (EF) was calculated for every trace metal.
162 The two concentration peaks observed at 1947 ± 11 for Ni (Figure 4) and Cr (Figure S4B)
163 correspond to a significant anthropogenic impact (EF = 2.0 for Ni). The EF and concentrations of
164 Hg (Figure 4) and other trace metals of group 3 (Figure S4C) progressively increased over time,
165 with maximum EF values between 1.9 and 9.5. These values demonstrated a moderate to severe
166 anthropogenic contamination after WWII in this order: Zn < Pb < Ag < Cu < Hg. This post-WWII
167 pollution dynamics was confirmed by Pb isotope ratios (Pb/Al, $^{206}Pb/^{207}Pb$, $^{206}Pb/^{208}Pb$, Figure 4,
168 Figure S4D, Figure S4E) and Polychlorinated biphenyl (PCB) contamination profiles (Figure 4).
169 The concentration profile of the sum of the seven PCB indicator congeners confirmed the influence
170 of higher anthropogenic input from the 1950s onward. Indeed, the concentration profile of the sum

of the seven indicator congeners showed a progressive increase in PCB contamination from 1958 ± 7 until the peak at 1981 ± 5 following the pattern of the third group of heavy metal (Figure 4).

During WWII the town of Brest was under Nazi occupation. Historical documents provide qualitative information about wartime activities linked to pollution, such as the construction of a submarine base, industrial army activity, navy traffic, and fuel deposit fires. Historical data are available about the quantity of bombs dropped on the town of Brest and its bay. The 30,000 tons of bombs and the 100,000 shells deployed over Brest during WWII and even more intensely during Ally liberation (Figure S1C) must have polluted the water either directly or indirectly through waste and detritus collected by river catchments flowing in the coastal waters of the bay. The metal composition of such bombs and explosives are imprecise or very difficult to retrieve. Yet, it is interesting that trace metal anomalies, including Pb and Cr, were found in sediment samples to be coincident with the Japanese aviation bombing of Pearl Harbour, the U.S. navy outpost during the WWII, on December 7, 1941[32].

Regarding the post-WWII period it is difficult to designate a particular source of metal contamination and the potential inputs could come from atmospheric depositions (Hg and Pb), agricultural phytosanitary products (Cu and Zn), and urban waste (polymetallic inputs). PCB contamination profiles sustain the hypothesis of contaminations of agricultural origin. from the 1950s onward. These profiles in sediment are similar to those of other French human impacted sites[33,34] or other agriculturally exploited sites[35,36]. A palynological study (pollen grains and dinoflagellate cysts) carried out on a twin core of the DE allowed direct comparison between the evolution of landscape, surface water, and human practices on Bay of Brest watersheds and corroborate the hypothesis of the postwar agriculture contamination[37]. Pollen and dinoflagellate cyst concentration analyses indicate changes in agricultural practices in the Bay of Brest. An increase in *Alnus* pollen grain concentrations and shifts between cysts of *Lingulodinium polyedra* and *Gonyaulax digitale* were synchronous with protist shifts shown in this study. These variations

have been associated with the evolution of agricultural practices and the increase in river flow loading due to the implementation of a new agricultural policy after 1945[37].

Plankton shifts have been evaluated on relatively short time scales since the majority of plankton long-term series have been initiated from the 1950 onward, with the exception of the Continuous Plankton Recorder Survey, which started in 1937[38]. Changes in plankton communities during the 1980s–90s were already observed in the Bay of Brest using microscopy counts. These shifts were associated with unbalanced nitrogen/phosphorus (N/P) ratios over time and in particular to the high concentrations of nitrogen in coastal water due to run-offs of agricultural field through water catchments and rivers[39,40]. To compensate for the gap in pre-industrial plankton data, researchers have used modeling approaches mostly to evaluate the effect of climate changes on plankton[41,42]. Traditional sedimentary paleoecological approaches based on microfossil analyses (spores, diatoms frustules, dinoflagellate cysts, foraminifers and coccoliths, and acritarchs) have allowed researchers to evaluate shifts on a paleoclimatological time scale, but also community changes after industrial pollution[37,43]. *Sed*aDNA analyses on plankton have shown its potential as a tool for studying the effect of human perturbation on biological communities[18,43,44,45,46]. Paleogenetic analyses revealed long-term shifts in plankton sometimes proving the anthropogenic influence[9,10,12,13,17], and the irreversibility of those changes[47,48]. *Sed*aDNA analyses have highlighted the increase and recrudescence of harmful algal bloom species in lakes[49] and coastal waters[7,8] and reflected an increase in eutrophication due to human pressures[9,10,13,17,48,50]. Our paleogenetic study showed that the cumulative effect of the trace metal and PCB pollution of the WWII and the postwar periods caused drastic changes in paleocommunity compositions, especially for dinoflagellates and stramenopiles, and the variations in dominant genera within these groups after the 1980s and 1990s. The effect of punctual or long-term contaminations from heavy metals (including Pb, Ni, and Cr) and PCBs are known to affect coastal plankton community composition[51,52] and to have a negative effect on phytoplankton species development[53], including

dinoflagellates[54,55]. The occasional and chronic human impacts occurred during the WWII and post-war period resulted in unstable and non-resilient variations of protistan communities the Bay of Brest over the last 70 years. Hence, this study demonstrates the potential irreversible consequence of multiple and cumulated pollutions over the microbial compartment of the coastal ecosystem.

What defines healthy coastal ecosystems is under debate. The main issue is whether natural systems are in balance and if they tend to return to that balance when perturbed or whether ecosystems are dynamic systems that are transient and unstable[1]. The bottleneck of such analysis is the contemporary acquisition of baselines of pristine ecosystem conditions and post-perturbation analyses. The comparative analysis of past versus modern ecosystem conditions may help to establish or optimize ecosystem strategies[4]. This study highlights the importance of retrospective analyses for the evaluation of coastal ecosystem stability and resilience and the relevance of paleogenetic data for these analyses. The impact of short- and long-term chronical pollution is demonstrated here on the microeukaryotic planktonic communities, a key compartment in marine ecosystems. Shifts in this compartment might cause cascading effects on other biological components of the ecosystem affecting the whole marine food web. These findings can further sustain the use of the paleoecological approach for the development of restoration efforts and policy actions aiming at a sustainable management of coastal areas.

Acknowledgments

Research funds were provided by the Brittany Region (Région Bretagne) as part of the *Paleoecology of* Alexandrium minutum *dans la Rade de Brest*–Marché n°2017-90292 project PALMIRA, which supported the core sampling, analyses, and post-doc fellowship of MLassudrie. Analyses were also funded by the initiative Ecosphere Continentale et COtière (EC2CO) of the *Institut National des Sciences de l'Univers/Centre Nationale de la Recherche Scientifique:* PALMITO (2013–2015) and CA'MOMI (2015–2017) projects. We thank Arnaud Marrec and

Yannick Fagon (Région Bretagne – Service Ingénierie de la Direction des Ports), who allowed the implementation and progression of PALMIRA. We are grateful to all members of the crew of the N/O *Thalia* ship of Ifremer for providing technical expertise in sediment core collection. We thank Angelique Roubi and Jérémie Gouriou of the laboratory GM/LGS of Ifremer for helping during onboard core sampling. We acknowledge our colleagues from the laboratory DYNECO/Pelagos and of Ifremer (Françoise Andrieux, Annie Chapelle, Cécile Jauzein, Mickaël Le Gac, Martin Plus, Sophie Schmitt, and Agnès Youenou) for their assistance during core subsampling. We are warmly grateful to Lauriane Madec (Ifremer), Khadidja Z. Klouch (a PhD student supervised by RS from 2012 to 2016), and Laure Guillou (CNRS, Station Biologique de Roscoff, France) for their initial contribution to the EE and DE core analyses. We thank Stéphane Lesbats and Olivier Dugornay of Ifremer's Audiovisual Service for onboard collection and scuba diving images of the sampling and for producing videos for the project. We thank colleagues from the Ifremer PFOM/LPI laboratory for having provided clean laboratory facilities and Darryl Perree for technical assistance in genetic analyses. We acknowledge the historical archive personnel of Brest and Quimper and in particular Hugues Courant, Isabelle Knab-Delumeau (Ecole Navale de Brest), and Yves Coativy (University of Brest) for their help in the analyses of historical information of the Bay of Brest. Muriel Vidal is acknowledged for her contribution to the rational and analysis of the work. We are warmly grateful to Isabelle Domaizon (INRAE) for helpful discussion during the entire project. R.S., M.L., and K.N.M. are part of GDR PHYCOTOX, a CNRS/IFREMER French national network on Harmful Algal Blooms.

Author contributions

R.S. designed and performed the research, conceived and carried out sampling, analyzed results and data, and wrote the paper. M.Lassudrie performed DNA extraction, genetic analyses, analyzed results, and contributed to writing. P.C., C.N., and L.Q. contributed to metabarcoding biostatistical

analyses. P.D. curated the data depositary. N.B. and V.L. performed, respectively, heavy metal and PCB analyses; analyzed results; and contributed to writing. S.S. carried out sediment dating and contributed to writing. A.E. helped in core sampling realization, carried out granulometry analyses, and contributed to writing. K.N.M., C.L., and A.P. contributed to paleoecological data analyses and interpretation. M.L. and J.Q. technically supported sampling and genetic analyses.

Declaration of interests

The authors declare no competing interests.

Figure legends

Figure 1. Paleocommunity diversity. Eukaryotic diversity composition of the BH core of the Bay of Brest inferred by metabarcoding of the V7 (left panel) and V4 (right panel) 18S rDNA of *sed*aDNA extracted from Medieval to contemporary sediments. Eukaryotic lineages are listed and color tones are used to indicate eukaryotic groups.

Figure 2. Shifts in dinoflagellate community composition. Dinoflagellate diversity analyses inferred from the V4 metabarcoding data of the TOT *sed*aDNA of the BH, DE, and EE cores of the Bay of Brest. Core dinoflagellate orders are identified with color tones (red: Gonyaulacales; yellow: Peridiniales; blue: Gymnodiniales; green: Suessiales; violet: Dinophysales). The dinoflagellate sister clades of marine alveolate (MALV) groups I, II, and III are also represented. Unidentified dinoflagellates are classified as Unknown. The multivariate regression tree analysis suggested dates of chronological partitioning of the data, representing shifts in community composition, and identified the dinoflagellate group mostly explaining these shifts. Only the first and major complexity level is represented. The

296 genus *Gonyaulax* (Gonyaulacales) is responsible for 100% of the deviance in the break point
297 identified in 1941 for BH (complexity: 35.6), for 43% of the deviance in the break point
298 identified in 1987 for DE (complexity: 42.1), and for 77% of the deviance in the break point
299 identified in 1998 for EE (complexity: 33.7). See also Figures S2 and S3.
300
301 **Figure 3. Shifts in stramenopile community composition.** Stramenopile diversity analyses
302 inferred from the V4 metabarcoding data of the TOT *sed*aDNA of the BH, DE, and EE cores
303 from the Bay of Brest. Stramenopiles groups are identified with color tones (red: phylum
304 Bacillariophyta [diatoms]; green: phylum Dictyochophyta; yellow: phylum Labyrinthulea;
305 blue: marine stramenopiles [MAST]; violet: Oomycota; other colors: clades with *incertae*
306 *sedis* classifications). Unidentified stramenopiles are classified as Unknown. The
307 multivariate regression tree analysis suggested dates of chronological partitioning of the
308 data, representing shifts in community composition, and the identified stramenopile group
309 mostly explains these shifts. Only the first and major complexity level is represented. The
310 diatom genus *Chaetoceros* is responsible for 93% of the deviance in the break point
311 identified in 1952 for BH (complexity: 19.5) and 100% of the deviance in the break point
312 identified in 1998 for EE (complexity: 33.7). The group MAST-12A is responsible for 100%
313 of the deviance in the break point identified in 1942 for DE (complexity: 63.0)
314
315 **Figure 4. Pollutant temporal variations.** Pb isotope ratio and selected heavy metal and PCB
316 concentrations in the BH core of the Bay of Brest. The Al-normalized dynamics of Li, Ni,
317 and Hg are representative of three groups of analyzed heavy metal. The cumulative
318 concentrations of the seven measured indicator PCB congeners (CB28, 52, 101, 118, 138,
319 153, 180) are indicated as Σ7PCBs. See also Figure S4.
320

STAR Methods section

Resources Availability

Lead Contact

Further information and requests for resources and reagents should be directed to and will be fulfilled by the Lead Contact, Raffaele Siano (raffaele.siano@ifremer.fr).

Materials availability

This study did not generate new unique reagents.

Data and code availability

All data needed to evaluate the conclusions of the paper are presented in the paper and/or in the Supplementary Material. Raw Illumina-Miseq data used for metabarcoding analyses have been submitted to NCBI (https://www.ncbi.nlm.nih.gov) with the data reference number PRJNA667629 (BH data) and PRJNA680674 (DE and EE data).

Experimental model

Study area

The Bay of Brest (Brittany, France, northeast Atlantic) is a semi-enclosed coastal ecosystem connected to the Iroise Sea (Atlantic Ocean) by a narrow (2 km) and deep (50 m) strait (Figure S1A). The bay is a shallow macrotidal coastal ecosystem with 50% of its surface deeper than 5 m. It is characterized by coarse sediments in deep waters and fine and muddy sediments in the upstream part of the estuaries. The majority (80%) of freshwater inputs come from two main rivers: the Aulne River (1842 km^2) in the southeastern part and the Elorn River (402 km^2) in the northeastern part of the Bay. The Brest area experienced a progressive development from the Antiquity through the

Middle Ages during the Duchy of Brittany, but it became a real naval town during from the XVIIth to XVIIIth centuries with the construction of the naval harbor. During this time, the population and the naval activity increased progressively. Then, after a lull of almost a century, Brest experienced a second industrial development from the end of the XVIIIth century until WWI. In 1940, the German army conquered Brest and built the famous submarine base in only three months. The base, the coastal area, and the whole town were bombed continuously by the Allies until 1945, with more than 30000 tons of bombs deployed (Figure S1C). The town of Brest was completely destroyed, with 965 people killed and 740 injured. During this period, the coastal area was the receptacle of heavy pollution due to the industrial army activity, navy traffic, and fires of French fuel deposits practiced by the German army on the land. The town of Brest was liberated on September 19, 1944, after 45 days of heavy fighting. After the liberation, the town and the harbor started their reconstruction. In 1947, the explosion of the Ocean Liberty vessel provoked grave damage to the entire town and the coastal area, with more than 3000 tons of the heavily explosive fertilizer ammonium nitrate released in the harbor's waters. Since 1950, the Brest area has undergone an intensive agricultural industrial development: the urban area increased and the harbor extended over the sea. During this period and until the 1990s, the area had experienced several changes in the anthropogenic loading of nutrients; with an increase in nitrogen supply due to the development of anthropogenic activities, and near the end of that period, a decrease in phosphorous supply resulting from the ban of washing powders containing orthophosphates[56]. Consequently, a significant imbalance in the nitrogen/phosphorus ratio[57] altered the composition of planktonic and benthic communities[39,40,58]. After the 1990s, the agricultural policy of the region has tried to control eutrophication of the area, and since then the nutrient loading has progressively decreased in the coastal area of the Bay of Brest.

Core sediment sampling

371 Biological analyses were inferred from three sediment cores collected in the Bay of Brest. Two
372 interface cores were collected by a gravity corer at the main estuaries' outlets of the Bay of Brest:
373 the Elorn Estuary (EE: 48°23'46.79"N, 4°23'2.01"W; December 11, 2012; 12 m depth; core length
374 31 cm) and the Daoulas Estuary (DE: 48°20'46.6"N, 4°17' 41.20"W; May 21, 2014; 3 m depth; core
375 length 58 cm) (Figure S1A). A third core was collected near the Brest Harbor in a non-dredged
376 zone (BH: 48°22'52.74"N, 04°26'54.60"W; April 25, 2017; 7.10 m depth; core length 344 cm) on-
377 board the N/O *Thalia* using a Kullenberg core sampler (Figure S1A; Video S1). Dating was
378 obtained from a twin core collected at the EE (see[7] for details of methods) and from the same cores
379 used for biological analyses at DE and BH. Immediately after sampling, sediment cores were
380 delicately extruded and sliced into 1 cm thick layers (Video S1). Due to its length, the BH core was
381 previously separated into four sections of equal length. For EE and DE interface cores, every 1 cm
382 layer was collected and analyzed. For the long BH core, only one in two slices was used for
383 subsampling and further analyses to avoid contamination across sample layers. To further avoid
384 contamination by smearing between layers during the core extraction, only the inner part of each
385 slice was subsampled, using sterile 6 cm diameter Petri dishes and sterilized wooden tongue
386 depressors (Video S1). Sterile, new equipment was used to sample each layer. Samples collected
387 in a Petri dish for genetic analyses (about 10 g of wet sediment) were preserved in plastic 50 mL
388 deoxygenated cryotubes, immediately frozen in liquid nitrogen, and then stored in a -80°C freezer
389 until further analyses. Samples for granulometry, organic carbon, heavy metals, and PCB
390 compounds were collected from the same layers of DNA samples, whenever possible, or from the
391 discarded layer not used for genetic analyses. For organic carbon analysis, samples were frozen at
392 -20°C and then lyophilized before analysis. Other sediment aliquots were stored at 4°C and in the
393 dark until further analysis.
394
395 **Method details**

Sediment dating and granulometry

Dating of recent sediments (< 150 years) was established for the Elorn Estuary (EE), Daoulas Estuary (DE) and Brest Harbour (BH, KS06) cores using depth profiles of excess ^{210}Pb ($^{210}Pb_{xs,}$ lead), a naturally-occurring radionuclide, and ^{137}Cs (cesium), an artificial radionuclide. The chronology of DE and EE were previously described by Klouch et al.[7]. The EE and DE cores covered, respectively, about 72 cal. yr. (calendar year) (from 1939 ± 2 to 2011 ± 1 AD) and 99 cal. yr. (from 1915 ± 7 to 2014 ± 1 AD) (Data S1A, Data S1B). The BH core is here described for the first time (Figure S1B, Data S1C) and covers the longest time period from 2928 ± 94 BC (4878 ± 94 BP) to 2015 ± 1 AD, i.e., about 5000 cal. yr.

For the BH core activities (mBq g^{-1}) of ^{210}Pb, ^{226}Ra (radium), and ^{137}Cs were measured in ~10 g of dry sediment using Broad Energy Germanium γ detector (BEGe, Mirion Technologies, France). The presence of shell fragments and maerl made gamma measurements difficult. First, the coarse carbonate fraction was sorted and removed. The remaining fine carbonate fraction diluted the radioelement contents, which implies long counting times ranging from 24 to 126 hours per sample. The detector was calibrated using certified reference material from the International Atomic Energy Agency (RGU-1; SOIL-6). Excess ^{210}Pb ($^{210}Pb_{xs}$) was calculated as the difference between the measured ^{210}Pb and ^{226}Ra activities. Activity errors were based on 1 SD counting statistics and propagated for $^{210}Pb_{xs}$. The two first layers of the core were measured twice a few days and several months after sampling to determine excess ^{234}Th (thorium), a short-lived radionuclide ($T_{1/2}$ = 24.1 days), which is a tracer of a good recovery of the uppermost sediment and of bioturbation. Activities of $^{210}Pb_{xs}$ present an exponential decrease from the top of the core to negligible values below 20 cm. This rapid decrease and the absence of a mixed layer in the upper section of the $^{210}Pb_{xs}$ profile testify to the absence of significant mixing of the sediment. The long-lived and naturally-occurring ^{232}Th is usually associated with the detrital fraction; therefore, the rather constant ^{232}Th activity in the BH core indicates the absence of changes in lithological sources or proportions. This implies

that the changes in $^{210}Pb_{xs}$ activities with depth are mainly related to time (radioactive decay of ^{210}Pb according to its half-life of 22.3 years) and are suitable to estimate sedimentation intensity.

The constant flux and constant sedimentation (CF–CS) model were used to calculate a mean sedimentation accumulation rate of 0.23 ± 0.040 cm yr^{-1} from the $^{210}Pb_{xs}$ profile. The DE and EE cores have higher mean sediment accumulation rates due to fluvial sediment inputs (EE: 0.44 cm yr^{-1}; DE: 0.41 cm yr^{-1}) than the BH core. For BH the ages of the sediment layers were calculated using the sedimentation rate and assuming the age of the top sediment to be 2015. The ^{137}Cs activities are low but present an onset at about 16 cm, which corresponds to the first introduction of this artificial radionuclide in the environment in the early 1950s and validates the chronological framework based on $^{210}Pb^{xs}$ (Figure S1B).

Dating of ancient sediments (> 150 years) for BH was performed by analyzing ^{14}C in eight gastropod shells (*Bittium* spp., *Crisilla* spp., *Hydrobia* spp., *Jujubinus* spp., and *Rissoa* spp.; total weight of each sample < 10 g) collected from the sieved sediment. The remaining material of five of these samples was not enough to perform genetic extractions. ^{14}C analyses were conducted at the Poznań Radiocarbon Laboratory (Poznań, Poland). Absolute dating was corrected for the mean ^{14}C age difference between the atmosphere and oceanic surface waters by applying a reservoir correction (R) of 325 years with an applied regional deviation (DR) for the bay of Brest of 46 years. The results of absolute dating were then calibrated using Calib Rev 7.0.4 software from the "Intcal13" calibration curve[59], with a confidence level of 95% for the SD (sigma 2). There was no dating inversion for the eight analyzed samples; however, the ^{14}C results showed two important time gaps in dating (Data S1C). The former concerns the gap between 32 and 82 cm below the seabed surface separating the recent sedimentation developed from the middle of the XIX^{th} century (1879 yr. ± 21 AD), estimated by ^{210}Pbxs, and old deposits dated from the central middle age (530 ± 108 AD to 874 ± 111 AD). Additional sediment analyses on other cores (data not shown) showed that this gap is less important and may have occurred between 1000 AD and 1350 AD. This time

offset is recorded for all the conserved sediment deposits in the bay of Brest. This period is well known to be a warm climatic sequence called the Medieval Warm Period (MWP) characterized by recurring winter successive storms[59], at the origin of the construction of aeolian dune systems on the North Atlantic Ocean coasts. The second time gap separates the Middle Ages from the Egyptian period, more precisely corresponding to the Third Intermediate Period until the Early Dynastic Period. It represents a seismic unconformity surface ranging from 2025 ± 129 BP to 3184 ± 164 BP[59] and corresponds to be a typical geological transition characterizing a precise step of the marine transgression and called the maximum flooding surface (MFS). The coarse deposits between 213 and 233 cm in the core associated with this time gap result of a high-energy marine environment that was able to erode underlying sand Egyptian age deposits.

For sediment granulometry, particle size analyses were carried out with a laser diffraction system for the sediment fraction below 2 mm. The percentages of the main sedimentary classes (gravel, sand, silt, and clay) were thus determined for each level sampled with the Gradistat package developed by Gregoire et al. (see[60] for methods). All cores mostly comprised a mix of clay, silt, and fine sand particles; the BH core was 4 ± 4% clay, 43 ± 9% silt, and 36 ± 8% fine sand particles (mean ± standard deviation [SD]). However, in the lower part of the BH core, below 204 cm, the sand and detritic gravel sediment fraction increased to represent more than 80% of the total sediment sampled.

_sed_aDNA extraction and amplification

Genomic DNA extraction was carried out from 3–10 g of wet sediment from each of the 31 and 58 layers, respectively, of the EE and DE cores, and from 46 layers of the BH core (Table S1). In marine sediments, given the importance of resting stages—which protect DNA inside the cells—it was hypothesized that intracellular DNA constitutes the highest proportion of the total *sed*aDNA extracted with classical protocols used for soil matrices, such as in the DNeasy PowerMax Soil Kit

(Qiagen). This hypothesis was tested on the BH samples. For each of the 46 sediment layers of BH, three different extraction protocols were applied to extract respectively: (1) total DNA (TOT) (DNeasy PowerMax Soil Kit as per the manufacturer instructions); (2) intracellular DNA (IN) from resting stages[61], by eliminating extracellular DNA through washing and heating steps before DNA extraction using the DNeasy PowerMax Soil Kit); and (3) extracellular DNA (EX) (following methods used in terrestrial ecological biodiversity surveys[24], which comprises extracting extracellular DNA in saturated phosphate buffer prior to using the DNeasy Power Max soil kit without the cell lysis step).

All *sed*aDNA extractions and manipulations were performed to avoid cross-contamination between samples or with modern DNA, by following specific instructions for working with aDNA and specifically for marine *sed*aDNA[5,22,62]. Extractions were carried out in an isolated, specific clean laboratory adapted to aDNA extraction, under a laminar flow cabinet (Video S1). One sediment layer was extracted at a time, all the surfaces and material used were carefully decontaminated between each sample treatment using chlorine or DNA-away™ (Thermo Fisher), and the laminar flow cabinet was also decontaminated with ultraviolet light. The analyst wore dedicated clothing and disposable personal protective equipment including a lab coat, gloves, and a facemask that were changed between each sample (Video S1). Blanks (no template controls) were extracted to check for the absence of contamination from the working area and from kit reagents. DNA extracts were immediately stored in a dedicated -80°C freezer. DNA was quantified with the Quant-iT™ PicoGreen® dsDNA assay (Invitrogen).

IN *sed*aDNA extractions yielded a DNA concentration close to that of total TOT *sed*aDNA extractions all along the BH core (Figure S2A, Figure S2B), whereas EX *sed*aDNA extractions yielded a constant, low DNA concentration all along the core (Figure S2A, Table S1). There were higher concentrations at superficial core layers in TOT and IN fractions (5 cm depth; max 4971.61 ng DNA g^{-1}), then a rapid decrease in concentrations down to 19 cm depth (max 761.64 ng DNA

g^{-1} in TOT). There were constant TOT and IN *sed*aDNA concentrations from 19 to 222 cm depth (respective averages ± standard deviation: 697 ± 135 and 566 ± 113 ng DNA g^{-1}). From 231 cm to the end of the core, TOT and IN *sed*aDNA concentrations decreased considerably (278 ± 80 and 239 ± 94 ng DNA g^{1}, Figure S2A). This section of the core corresponded to coarser (sandy) sediment granulometries compared with the rest of the core. Such a sediment type is less favorable to DNA preservation, which probably explains the DNA concentration drop observed in this part of the core (Figure S2A). In the light of results obtained for these samples, only the total DNA extraction protocol was used for EE and DE extractions. The comparison of different DNA extraction methods showed that the DNA concentrations in sediments along the BH core were similar when comparing total *sed*aDNA (TOT) and intracellular *seda*DNA (IN) extracts, whereas the concentration was much lower in the extracellular *sed*aDNA (EX) extracts (Table S1).

To analyze possible *sed*aDNA degradation by fragmentation and to check the possibility and reliability of the amplification of > 300 bp DNA fragments from ancient marine sediments, metabarcoding analyses of the V4 (ca. 390 bp) and V7 (ca. 260 bp) hyper-variable regions of the 18S rRNA gene were compared for BH samples. The V4 region is commonly used in protist biodiversity survey[27,50], whereas the V7 barcode has been suggested as a useful paleogenetic barcode in paleolimnological studies[13], although it had not been tested in marine paleogenetic approaches. The V4 and V7 regions were amplified in samples and extraction using respectively the eukaryotic primers TAReuk454FWD1 and TAReukREV3[27] and 960F et NSR1438[13] assembled with the GeT-PlaGe adaptors from GeT sequencing platform (Toulouse, France, http://get.genotoul.fr) for Illumina Mi-Seq sequencing. For both amplifications, the reaction mixture was prepared in a final volume of 50 µL, containing 0.02 U $µL^{-1}$ Phusion High Fidelity DNA polymerase and 1X Phusion High-Fidelity Buffer (NEB), 0.2 mM dNTP mix, 0.4 µM of each primer, 3% dimethyl sulfoxide, 2 µL DNA template, and DNA-free water. Extraction blanks were also amplified, and positive controls (mock protist community composed of five different species

of microalgae) and negative controls (without DNA templates) were used to check the efficiency and specificity of the PCR. The following cycling program was used for V4: an initial denaturation step at 98°C for 30 s, 14 cycles of 98°C for 10 s, 53°C for 30 s, and 72 °C for 30 s; 21 cycles of 98°C for 10 s, 48°C for 30 s, and 72°C for 30 s; and a final elongation step at 72°C for 10 min. The cycling program for V7 was: an initial denaturation step at 98°C for 30 s; 35 cycles of 98°C for 10 s, 55°C for 30 s, and 72°C for 30 s; and a final elongation step at 72°C for 10 min. PCR products were checked on a 1.5% agarose gel (1× Tris-borate-ethylenediaminetetraacetic acid and Gel Red). Three replicates reactions per sample were run and PCR products were pooled and sent to GeT sequencing platform, where they were purified and checked for quality and quantity using a fragment analyzer. PCR products yielding an insufficient DNA concentration of the expected fragment size were excluded (extraction blanks, 3 EE samples, 27 DE samples, 7 EX DNA, and 1 IN DNA for the V4 region in BH samples). Four libraries were built, keeping separate the samples from different cores and the different regions (V4 and V7), for sequencing from both sides using an Illumina MiSeq (2 × 250bp for V4 and 2 × 150bp for V7). As for the BH core, for the V4 region the range number of reads obtained after sequencing were: 13 812 to 143 391 (TOT), 32 487-118 101 (IN), and 7 566-129 794 (EX). For the V7 region the range number were: 2 585 to 72 950 (TOT), 1 795-73 061 (IN), and 997-112 916 (EX). For the EE and the DE core the V4 read number range were respectively: 32 734-425 286 and 37 471-236 421.

Metabarcoding analyses

Sequenced data of the V4 (BH, DE and EE) and V7 (BH) 18S rDNA were submitted to quality checking by FastQC coupled with MultiQC. Primers and adapters have been removed in forward and reverse file separately with Cutadapt v1.18[63] using the "--discard-untrimmed" argument, which discards reads without target primers. BBmap v38.22 was used to reorder reads and eliminate singletons from each pair with the repair function. Sequence filtering and trimming as well as

546 Amplicon Sequence Variant (ASV) inference were carried out using the DADA2 strategy with the
547 DADA2 R package and using the default parameters[64]. Taxonomic assignment of ASV was
548 performed on the basis of the naive Bayesian RDP methodology with the database PR^2 v4.11[65].
549 Finally, metadata files (sample ID, sediment layer dept, type of DNA extraction, and taxonomy)
550 was separately created for each sediment core (BH, DE, and EE). There was a second data cleaning
551 to remove ASVs identified as contamination (e.g., ASVs assigned to *Homo sapiens* or *Capra*
552 *hircus*). For diversity and ecological studies, ASVs with relative abundances < 0.0% for the V4
553 dataset and < 0.006% for the V7 dataset were removed from the databases using the R package
554 phyloseq. This step allowed us to eliminate rare ASVs and further sequence errors and to analyze
555 > 90% of total ASV richness for each database (Table S2). After this step, samples 1-4 (6 cm depth)
556 and 1-6 (8 cm) of the BH core were eliminated from the V4 and V7 database because the observed
557 richness value was too low. To compare samples, V4 and V7 data of all cores were normalized by
558 a rarefaction method, which comprises a random subsampling of the data by a hypergeometric law.
559 A normalization threshold was established on the basis of rarefaction curves (Figure S2F) modeled
560 using the function ggrare deriving from the function rarecurve of the vegan R package with the
561 argument "step=100"[66]. The phyloseq R package rarefy_even_depth was used for data
562 normalization[67]. For BH, only samples from the surface to 231 cm, used for diversity and ecological
563 analyses, were normalized. For DE and EE, all samples were normalized.

564 Comparative diversity patterns emerged between TOT and IN with both V7 and V4 18s
565 rDNA β diversity analysis. For both barcodes, the highest number of ASV were found (in both
566 absolute number and percent over the total ASV number) with the IN DNA extraction method,
567 throughout the whole core (Table S2). The highest ASV number (both in absolute number and
568 percent over the total ASV number) were found in the middle section of the core (from 148 to 160
569 cm) during the Middle Ages (Figure S2C). There were progressive decreases in diversity toward
570 the upper section of the core (more recent times) and the deeper layers (more ancient times) (Figure

S2C). Sample assemblages (β diversity, analysis based on the Jaccard diversity index) were similar between TOT and IN. EX samples differed in ASV composition (Figure S2D). Embryophyta (plants) and Unknown ASVs were preferentially amplified in EX samples. BH sediment sample layers could be separated into two groups according to both amplicon sequence variant (ASV) richness and β diversity the first including layers from 2 to 231 cm, and the second composed of deeper core layers, from 233 to 340 cm, with lower ASV richness (Figure S2D). The rarefaction curves for each sample showed different TOT and IN richness saturation according to the core layer depth (Figure S2F). The decrease in ASV diversity and DNA concentration in the lower part of the core was associated with a different sediment granulometry. *Sed*aDNA likely had been better preserved in the silty–muddy sediments of the upper part of the core than in the coarse sediments of the lower part. Given these differences, we could not compare the DNA archives of the lower part of the BH core (233–340 cm) to the more recent ones. Therefore, we performed further analyses of protist diversity using normalized data from the upper part of the core only (3–231 cm), which covered a period of ca. 1400 years (including the Anthropocene period), from the Middle Ages (V^{th}–VI^{th} centuries) to the contemporary era (XXI^{th} century).

Most of the ASV obtained with the TOT *sed*aDNA extraction method were common to those obtained with the IN *sed*aDNA when considering the ≥ 1% abundant protist ASVs, with on average 69% and 58% of TOT ASVs common to IN when using the V7 and V4 barcodes, respectively (Figure S2E). These values increased to 76% (V7) and 65% (V4) when considering only ASVs from the surface to 231 cm (Figure S2E). In the lowest part of the core most of the ASVs that are not in common between IN and TOT were only amplified with TOT extraction method. Over the entirety of the core, 83% (V7) and 82% (V4) of these common ASVs were assigned to protist genera known to include species that can produce resting stages (Data S2).

Pollutant analyses

596 Heavy metal and PCB analyses were carried out on 12 sediment samples of the BH core, covering
597 the period of the industrial revolution of the XIXth century to contemporary times (AD 2003 ± 2).
598 Pollutant analyses were carried out on the same samples used for genetic analyses when enough
599 material was available. Whenever necessary, additional samples of lower or upper sediment layers
600 were exploited. For heavy metals, further control analyses were performed on more ancient
601 sediments. All reagents, labware acid cleaning, and solution dilutions for elemental and isotope
602 analyses were performed using 18.2 MΩ.cm^{-1} H_2O (Nanop System®) and ultra-pure acids
603 (PlasmaPure Plus grade, SCP science®). Unsieved dry aliquots of sediments were digested in
604 Teflon® bombs on a coated graphite block using a multiple-step acid procedure with hydrofluoric
605 acid, hydrochloric acid, and nitric acid. The final extract solution was split for subsequent elemental
606 and isotope analyses. Procedural blanks and international certified reference materials (MESS-3
607 from NRC – CNR®) were processed in each batch of sediment samples and followed the complete
608 procedure (digestion, elemental analysis and isotope measurements). Elemental concentrations of
609 Ag, Al, Cd, Co, Cr, Cu, Fe, Hg, Li, Mn, Ni, Pb, V, and Zn were determined by inductively coupled
610 plasma mass spectrometry (Q-ICP-MS, iCAP Q, Thermo Fisher Scientific). The accuracy,
611 indicated by average bias, was always within 10% of the certified values of reference material for
612 the considered elements. The Pb isotope ratio ($^{206}Pb/^{207}Pb$ and $^{206}Pb/^{208}Pb$) measurements were
613 performed with the same Q-ICP-MS equipment. Mass bias and instrumental drift were corrected
614 with a standard bracketing method using the NIST SRM-981 standard reference material. The
615 $^{206}Pb/^{207}Pb$ and $^{206}Pb/^{208}Pb$ internal relative SD averages were 0.15 ± 0.05% and 0.47 ± 0.13% (1s,
616 n = 20), respectively.

617 To compare particle results from different locations with variable physical and chemical
618 composition, a normalization procedure is commonly applied. The dilution effects related to grain
619 size and mineralogical heterogeneities were decreased by the normalization of the Al concentration
620 in the sample to the concentration of a reference element. Al was used as the reference element for

621 the particulate material due to (i) its conservative behavior in the core; (ii) its characterization of
622 the clay-size fraction, which is enriched with most trace elements; and (iii) its very low sensitivity
623 to human activities. Normalized metal concentrations were obtained by dividing the concentration
624 of the studied element by the concentration of a normalizer element in the same sample (X in
625 Equation 1). Normalization to Al is widely used as a "proxy" of the clay content, generally
626 representative of the finest and more efficient fraction for element sorption. The reference
627 ([Element]/[X]) represents the local background determined as the concentration ratio considered
628 as free of anthropogenic influence.

629 Three heavy metal profile groups were identified in the sediment samples analyzed of the
630 BH core. Group I includes Li (Figure 4), V, and Cd (Figure S4A); group II includes Ni (Figure 4)
631 and Cr (Figure S4B); and group III includes Hg (Figure 4), Ag, Co, Cu, Mn, Pb, and Zn (Figure
632 S4C). Elements of the first group were closely related to Al concentrations and the dynamics of the
633 normalized concentrations were constant with mean ± SD values of 12.9 ± 0.8 mg kg^{-1} for Li, 19.8
634 ± 1.0 mg kg^{-1} for V, and 0.046 ± 0.007 mg kg^{-1} for Cd (Figure 4, Figure S4A). The elements of the
635 second group, Cr and Ni, had constant normalized concentrations along the core with values of 13.9
636 ± 0.6 mg kg^{-1} and 4.8 ± 0.2 mg kg^{-1}, respectively. There were two peaks of normalized
637 concentrations in the years 1947 ± 11 and 1913 ± 16 with an increase in concentrations up to 50%
638 (20.4 mg kg^{-1} for Cr (Figure S4B) and 9.8 mg kg^{-1} for Ni, Figure 4). Elements of the third group
639 had increasing normalized concentrations from 1958 ± 9 to more recent times (surface layers)
640 (Figure 4, Figure S4C).

641 The natural background was established using the lowest element/Al concentration ratios in
642 the core (38–39 cm depth). The relative enrichment factor (EF) of trace metals was used as an index
643 to estimate the degree of anthropogenic contamination:

644 Equation 1: EF = ([Element]sample/[X]sample) / ([Element]reference/[X]reference).

Many pollution classes have been defined for EF values. Considering the low variability of the local background and following previous class, we assumed: EF values < 1.5 representing no or minimal anthropogenic enrichment; values between 1.5 and 3 representing a moderate anthropogenic signature; values between 3 and 10 indicating a moderately severe anthropogenic contribution; and values >10 underlining a severe anthropogenic impact. Every trace metal element measured in the core before 1902 ± 17 had an EF < 1.5, representing minimal anthropogenic enrichment, except for Hg, which showed a higher EF (1.7). The two concentration peaks observed at 1947 ± 11 for Cr and Ni (Figure 4, Figure S4B) correspond to a significant anthropogenic impact (EF = 2.0 for Ni). After 1947 ± 11, the pattern of normalized concentrations and associated EF remained low for some elements. The EF was mainly between 0.9 and 1.5; the relatively low concentrations of Li, V, Co, and Cd over the whole profile demonstrated that these elements are mainly from a lithogenic origin and that there was no significant anthropogenic source for these elements. The EF and concentrations of others trace metals (Ag, Cu, Hg, Pb, and Zn) progressively increased over time, with maximum EF values between 1.9 and 9.5. These values demonstrated a moderate to severe anthropogenic contamination in the order Zn < Pb < Ag < Cu < Hg.

Given that ordinary chemical reactions will not cause variations in the isotopic composition of Pb, it has been demonstrated that Pb is a powerful tracer of sources. To assess the origin of Pb in the sediment of the BH core, we used isotopic compositions as pertinent tools (Figure 4, Figure S4D, Figure S4E). Normalized Pb concentrations in the sediment core showed constant values (3.4 ± 0.1 mg kg^{-1}) from 40.5 to 18.5 cm depth (Figure S4D) with constant $^{206}Pb/^{207}Pb$ (0.483 ± 0.001) (Figure 4, Figure S4D) and $^{206}Pb/^{208}Pb$ (1.198 ± 0.002) ratios (Figure S4D). Those ratios could be considered as the natural local background ratios, which is consistent with natural Pb isotope signatures referred to in previous studies performed in France coastal areas ($^{206}Pb/^{207}Pb$ natural = 1.195). At 1924 ± 14, a light peak of normalized Pb concentrations is observed correlated with a slight decrease of $^{206}Pb/^{208}Pb$ ratio (1.190 ± 0.002) (Figure S4D). At 1936 ± 12, a light peak of

$^{206}Pb/^{207}Pb$ corresponded to the World War II period (Figure 4). Across more recent times, $^{206}Pb/^{207}Pb$ and $^{206}Pb/^{208}Pb$ reached a natural local background ratio and normalized Pb concentrations increased more than threefold (Figure S4D). Concomitant variations in Pb concentrations and isotopes ratios showed the importance of anthropogenic activities and inputs in the Pb environmental cycle (Figure S4E).

The solvents (n-hexane, n-pentane, acetone, and iso-octane) used for Polychlorinated biphenyl (PCB) analyses were of trace analysis grade and supplied by SDS (France). PCB analyses were performed as described by Horri et al.[68,69]. Briefly, PCBs were analyzed by pressurized liquid extraction with the SpeedExtractor E-914 (Buchi Lab., Switzerland). The sulfur co-extracted with the organic compounds was removed using a tetrabutylammonium sulfite treatment before sequential purification with concentrated sulfuric acid and by adsorption chromatography on a Florisil column. The purified extracts were analyzed using gas chromatography with electron capture detection (GC-µECD, Agilent 7890B) equipped with two injectors, two columns (CP-Sil 19 and HT08, Chrompack), and two electron capture detectors (µECD Ni63). Among PCBs, the seven indicator PCB congeners were measured (CB28, 52, 101, 118, 138, 153, and 180), their sum being given as Σ7PCBs. A few other congeners were also analyzed to describe a larger range of chlorination from 3 to 8 chlorine molecules (CB31, 44, 49, 105, 110, 128, 132, 149, 156, 170, 187, and 194) to check the appropriate resolution of the gas chromatography system, and because they can highlight underlying mechanisms acting on the distribution of organic contaminants. Analytical blanks were systematically measured every six samples. The blanks were about 0.2 pg μl^{-1}, twentyfold less than the concentrations of the lowest standard of CB153 (i.e., < 0.1 ng g^{-1}), and much less for other determinants. Finally, six replicates of a reference material (BCR-SRM1491b) were analyzed to determine the accuracy and precision of the method. PCB recoveries varied between 77% and 115%. Hydrophobic and persistent organic contaminants such as PCBs have a particular affinity for the organic material and differences in the sediment organic fraction can lead

to differences in contamination levels. Therefore, to overcome these differences and to compare the different fractions, a standardization procedure was applied and the PCB concentrations were expressed per g of organic carbon in dry sediment[68].

Historical archive documentation

The departmental archives of Brest were consulted to find data, video, and pictures about the anthropic activities and events that occurred in the Bay of Brest that could have caused any pollution in the harbor area. In particular the, documents were analyzed concerning WWII (Figure S1C) and the Ocean Liberty vessel explosion. Some qualitative (videos, pictures) and quantitative (number of bombs per year, contents of the Ocean Liberty vessel) data were considered for the interpretation of shifts of the paleocommunities.

Quantification and Statistical Analysis

α (intraspecific) and β (interspecific) diversity and the diversity index were calculated using the vegan R packages Dplyr and Tidyr of R v3.4.4[70]. α diversity analyses were used to discriminate observed richness patterns in the BH core for all *sed*aDNA extraction methods (TOT, IN, and EX) Table S3). A non-metric multi-dimensional (NMDS) analysis inferred from a dissimilarity matrix based on the Jaccard index was carried out to analyze β diversity among TOT, IN, and EX samples of the BH core (Figure S2D). After the NMDS analysis, the ANOSIM test was performed to identify statistically similar groups of samples. Plots were created using the ggplot2 R package[71].

A chronological clustering of the BH, DE, and EE samples was performed to detect the dates and the hierarchical order of modification in the ASV paleocommunity structure. Prior to this analysis, relative abundances of ASV taxonomically assigned to the same genera/groups were cumulated. This cumulated ASV was named with the genus and/or taxonomic groups to which it belongs (according to PR^2 annotation). ASV not assigned to any species or genera assigned were

cumulated in a group named Unknown. For simplicity, in the Results section the taxonomic name of the genus or groups is used to indicate the cumulated ASVs. Separate MRT analyses[72] were performed on the protist, dinoflagellate, and stramenopile cumulated ASV data from the BH, DE, and EE samples. This time-constrained analysis was performed according to the instructions proposed by Bocard et al.[73], and the size of each tree was selected using the graphs of the relative error. The R package mvpart was used for this analysis. MRT level 1 is shown in Figure 2, Figure 3, and Figure S3.

Supplementary information

Data S1. Dating of Elorn Estuary (EE), Daoulas Estuary (DE), and Brest Harbor (BH) cores Related to STAR Methods.. **A)** Elorn Estuary (EE) sediment chronology. **B)** Daoulas Estuary (DE) sediment chronology. **C)** Brest Harbor (BH) sediment chronology.

Data S2. Taxa known to form resting stages for the. Related to STAR Methods. **A)** V7 barcode. **B)** V4 barcode.

Video S1. Core sampling, *in situ* and lab work on sediment cores. Related to STAR Methods.

References

1. Tett, P., Gowen, R.J., Painting, S.J., Elliott, M., Forster, R.,. Mills, D.K, Bresnan, E., Capuzzo, E., Fernandes, T.F., Foden, J., Geider, R.J., Gilpin, L. C., Huxham, M., McQuatters-Gollop, A.L, Malcolm, S.J., Saux-Picart, S., Platt, T., Racault, M.-F., Sathyendranath, S., van der Molen, J., and Wilkinson, M. (2013). Framework for understanding marine ecosystem health. Mar. Ecol. Prog. Ser. *494*, 1–27.

744 2. Waters, C.N., Zalasiewicz, J., Summerhayers, C., Barnosky, A.D., Poirier, C., Galuszka,
745 A., Cearretz, A., Edgeworth, M., Ellis, E.C., Ellis, M., Jeandel, C., Leinfelder R., McNeill,
746 J.R., deB Richter, R., Steffen, W., Vidas, D., Wagreich, M., Williams, M., Zhisheng, A.,
747 Grinevald, J., Odada, E., Oreskes, N., and Wolfe, A.P. (2016). The Anthropocene is
748 functionally and stratigraphically distinct from the Holocene. Science *351* aad2622.
749 3. Jonkers, L., Hillebrand, H., and Kucera, M. (2019). Global change drives modern plankton
750 communities away from the pre-industrial state. Nature *570*, 372–375.
751 4. Fordham, D.A., Jackson, S.T., Brown, S.C., Huntley, B., Brook, B.W., Dahl-Jensen, D.,
752 Gilbert, M.T.P., Otto-Bliesner, B.L., Svensson, A., Theodoridis, S., Wilmshurst, J.M.,
753 Buettel, J.C., Canteri, E., McDowell, M., Orlando, L., Pilowsky, J., Rahbek, C., and
754 Nogues-Bravo, D. (2020). Using paleo-archives to safeguard biodiversity under climate
755 change. Science *369*, eabc5654.
756 5. Boere, A.C., Sinninghe Damsté, J.S., Rijpstra, W.I.C., Volkman, J. K., and Coolen, M.J.L.
757 (2011). Source-specific variability in post-depositional DNA preservation with potential
758 implications for DNA based paleoecological records. Org. Geochem. *42*, 1216–1225.
759 6. Coolen, M.J.L (2011) 7000 years of *Emiliania huxleyi* viruses in the Black Sea. Science
760 *333*, 451–452.
761 7. Klouch, K.Z., Schmidt, S., Andrieux-Loyer, F., Le Gac, M., Hervio-Heath, D., Qui-Minet,
762 Z.N., Quéré, J., Bigeard, E., Guillou, L., and Siano, R. (2016). Historical records from dated
763 sediment cores unveiled the multidecadal dynamics of the toxic dinoflagellate *Alexandrium*
764 *minutum* in the Bay of Brest (France). FEMS Microbiol. Ecol. *92*, fiw101
765 8. Konkel, R., Toruńska-Sitarz, A., Cegłowska, M., Ežerinskis, Ž. Šapolaitė, J., Mažeika, J.,
766 and Mazur-Marzec, H. (2020). Blooms of toxic cyanobacterium *Nodularia spumigena* in
767 Norwegian fjords during Holocene warm periods. Toxins *12*, 257.

9. Stoof-Leichsenring, K.R., Epp, L.S., Trauth, M.H., and Tiedemann, R. (2012). Hidden diversity in diatoms of Kenyan Lake Naivasha: a genetic approach detects temporal variation. Mol. Ecol. *21*, 1918–1930.
10. Coolen, M.J.L., Orsi, W.D., Balkema, C., Quince, C., Harris, K., Sylva, S.P., Filipova-Marinova, M., and Giosan, L. (2013). Evolution of the plankton paleome in the Black Sea from the Deglacial to Anthropocene. PNAS *110*, 8609–8614.
11. Lejzerowicz, F., Voltsky, I, and Pawlowski, J. (2013). Identifying active foraminifera in the Sea of Japan using metatranscriptomic approach. Deep Sea Res. Part II: Topical Studies in Oceanograph *86–87*, 214–220.
12. Hou, W., Dong, H., Li, G., Yang, J., Coolen, M.J.L., Liu, X., Wang, S., Jiang, H., Wu, X., Lian., B., and Wan, Y. (2014). Identification of photosynthetic plankton communities using sedimentary ancient DNA and their response to late-Holocene climate change on the Tibetan Plateau. Sci. Rep. *4*, 6648.
13. Capo, E. Debroas, D., Arnaud, F., Guillemot, T., Bichet, V., Millet, L., Gauthier, E., Massa, C., Develle, A.-L., Pignol, C., Lejzerowicz, F., and Domaizon, I. (2016). Long-term dynamics in microbial eukaryotes communities: a palaeolimnological view based on sedimentary DNA. Mol. Ecol. *25*, 5925–5943.
14. Giosan, L., Orsi, W.D., 2,3, Coolen, M.J.L., Wuchter, C. Dunlea, A.G., Thirumalai, K., Munoz, S.E., Clift, P.D., Donnelly, J.P., Galy, V., and Fuller, D.Q. (2018). Neoglacial climate anomalies and the Harappan metamorphosis. Clim. Past *14*, 1669–1686.
15. More, K.D., Orsi, W.D., Galy, V., Giosan, L., He, L., Grice, K., and Coolen, M.J.L. (2018). A 43 kyr record of protist communities and their response to oxygen minimum zone variability in the Northeastern Arabian Sea. Earth Planet. Sci. Lett *496*, 248–256.

16. De Schepper, S., Ray, J.R., Sandnes Skaar, K., Sadatzki, H., Ijaz, U, Z., Stein, R., and Larsen, A. (2019). The potential of sedimentary ancient DNA for reconstructing past sea ice evolution. ISME J. *13*, 25566–2577.

17. Capo, E., Rydberg, Tolu, J., Domaizon, I., Debroas, D., Bindler R., and Bigler, C. (2019). How does environmental inter-annual variability shape aquatic microbial communities? A 40-year annual record of sedimentary DNA from a boreal lake (Nylandssjön, Sweden). Front. Ecol. Evol. *7*, 245.

18. Keck, E., Millet, L., Debroas, D., Etienne, D., Galop, D., Rius, D., and Domaizon I. (2020). Assessing the response of micro-eukaryotic diversity to the Great Acceleration using lake sedimentary DNA. Nature Comm. *11*, 3831.

19. Pomeroy, L. R. (1974). The ocean's food web, a changing paradigm. BioScience *24*, 499–504.

20. Azam, F., Fenchel, T., Field, J.G., Gray, J.S., Meyer-Reil, L.A., and Thingstad, F. (1983). The ecological role of water-column microbes in the Sea. MEPS *10*, 257–263.

21. Worden, A.Z., Follows, M.J., Giovannoni, S.J., Zimmernam, A.E., and Keeling, P.J. (2015) Rethinking the marine carbon cycle: Factoring in the multifarious lifestyles of microbes. Science *347*, 1257594

22. Armbrecht, L.H., Coolen, M.J.L., Lejzerowicz, F., George, S.C., Negandhi, K., Suzuki, Y., Young, J., Foster, N.R., Armand, L.K., Cooper, A., Ostrowski, M., Focardi, A., Stat, M., Moreau, J.W., and Weyrich, L.S. (2019). Ancient DNA from marine sediments: Precautions and considerations for seafloor coring, sample handling and data generation. Earth Sci. Rev. *196*, 102887.

23. Taberlet, P., Coissac, E., Hajibabaei, M., and Rieseberg, L.H. (2012). Environmental DNA. Mol. Ecol. *21*, 1789–1793.

24. Zinger, L., Chave, J., Coissac, E., Iribar, A., Louisanna, E., Manzi, S., Schilling, V., Schimann, H., Sommeria-Klein, G., and Taberlet, P. (2016). Extracellular DNA extraction is a fast, cheap and reliable alternative for multi-taxa surveys based on soil DNA. Soil. Biol. Biochem. *96*, 16–19.

25. Leander, B.S., Lloyd, S.A.J., Marshall, W., and Landers, S.C. (2006). Phylogeny of Marine Gregarines (Apicomplexa) — *Pterospora*, *Lithocystis* and *Lankesteria* — and the Origin(s) of Coelomic Parasitism. Protist *157*, 45–60.

26. de Vargas, C., Audic, S., Henry, N., Decelle, J., Mahé, F., Logares, R., Lara, E., Berney, C., Le Bescot, N., Probert, I., Carmichael, M., Poulain, J., Romac, S., Colin, S., Aury, J.M., Bittner, L., Chaffron, S., Dunthorn, M., Engelen, S., Flegontova, O., Guidi, L., Horak, A., Jaillon, O., Lukes, J., Malviya, S., Morard, R., Mulot, M., Scalco, E., Siano, R., Vincent, F., Zingone, A., Dimier, C., Picheral, M., Searson, S., Kandels-Lewis, S., Acinas, S. G., Bork, P., Bowler, C., Gorsky, G., Grimsley, N., Hingamp, P., Iudicone, D., Not, F., Ogata, H., Pesant, S., Raes, J., Sieracki, M., Speich, S., Stemman, L., Sunagawa, S., Weissenbach, J., Wincker, P., Karsenti, E., and Tara Oceans Expedition, Tara Oceans Coordinators (2015). Eukaryotic plankton diversity in the sunlit global ocean. Science *348*, 1–12

27. Ramond, P., Sourisseau, M., Simon, N., Sarah, R., Schmitt, S., Rigaut-Jalabert, F., Henry, N., de Vargas, C., and Siano, R. (2019). Coupling between taxonomic and functional diversity in protistan coastal communities. Environ. Microbiol. *21*, 730–749.

28. Forster, D., Dunthorn, M., Mahé, F., Dolan, J., Audic, S., Bass, D., Bittner, L., Boutte, C., Christen, R., Claverie, J.-M., Decelle, J., Edvardsen, B., Egge, E., Eikrem, W., Gobet, A., Kooistra, W.H.C.F., Logares, R., Massana, R., Montresor, M., Not, F., Ogata, O., Pawlowski, J., Pernice, M., Romac, S., Shalchian-Tabrizi, K., Simon, N., Richards, T., Santini, S., Sarno, D., Siano, R., Vaulot, D., Wincker, P., Zingone, A., de Vargas, C., and

839 Stoeck, T. (2016). Benthic protists: the under-charted majority. FEMS Microbiol. Ecol. *92*,
840 fiw120.
841 29. del Campo, J., Heger, T., Rodriguez-Martinez, R., Worden, A.Z., Richards, T.A., Massana,
842 R., and Keeling, P.J. (2019). Assessing the diversity and distribution of apicomplexans in
843 host and free-living environments using high-throughput amplicon data and a
844 phylogenetically informed reference framework. Front. Microbiol. *10*, 2373.
845 30. Mahé, F., de Vargas, C., Bass, D., Lucas, C., Stamatakis, A., Lara, E., Singer, D., Mayor,
846 D., Bunge, J., Sernaker, S., Siemensmeyer, T., Trautmann, I., Romac, S., Berney, C.,
847 Kozlov, A., Mitchell, E.A.D., Seppey, C.V.W., Egge, E., Lentendu, G., Wirth, R., Trueba,
848 G, and Dunthorn, M. (2017). Parasites dominate hyperdiverse soil protist communities in
849 Neotropical rainforests. Nat. Ecol. Evol. *1*, 0091.
850 31. Massana, R., del Campo, J., Sieracki, M. E., Audic, S., and Logares, R. (2014). Exploring
851 the uncultured microeukaryote majority in the oceans: reevaluation of ribogroups within
852 stramenopiles. ISME J. *8*, 854–866.
853 32. Ashwood, T.L., and Olsen, C.R. (1988). Pearl Harbour bombing attack: a contamination
854 legacy revealed in the sedimentary record. Mar. Pollut. Bull. *19*, 68–71.
855 33. Dendievel, A.-M., Mourier, B., Coynel, A., Evrard, O., Labadie, P., Ayrault, S., Debret, M.,
856 F. Koltalo, Copard, Y., Faivre, Q., Gardes, T., Vauclin, S., Budzinski, H., Grosbois, C.,
857 Winiarski, T., and Desmet, M. (2020). Spatio-temporal assessment of the polychlorinated
858 biphenyl (PCB) sediment contamination in four major French river corridors (1945–2018),
859 Earth Syst. Sci. Data *12*, 1153–1170.
860 34. Castro-Jiménez, J., Deviller, G., Ghiani, M., Loos, R., Mariani, G., Skejo, H., Umlauf, G.,
861 Wollgast, J., Laugier, T., Héar-Moisan, K., Léauté, F., Munschy, C., Tixier, C., and
862 Tronczyński, J., (2008). PCDD/F and PCB multi-media ambient concentrations, congener

patterns and occurrence in a Mediterranean coastal lagoon (Etang de Thau, France). Environ. Pollut. *156*, 123–135.

35. Elsenrelch, S., Capel, P.D., Robbins, J.A., and Bourbonniere, R. (1989). Accumulation and diagenesis of chlorinated hydrocarbons in lacustrine sediments. Environ. Sci. Technol. *23*, 1116–1126.
36. Schneider, A. R., Stapleton, H. M., and Baker, J. E. (2001) Recent declines in PAH, PCB, and toxaphene levels in the northern great lakes as determined from high resolution sediment cores. Environ. Sci. Technol. *35*, 3809–3815.
37. Lambert, C., Penaud, A., Vidal, M., Klouch, K.Z., Gregoire, G., Ehrhold, A., Eynaud, F., Schmidt, S., Ragueneau, O., and Siano R. (2018). Human-induced river runoff overlapping natural climate variability over the last 150 years: Palynological evidence (Bay of Brest, NW France). Glob. Planet. Change *160*, 109–122.
38. Batten, S.D., and Burkill, P.H. (2010). The Continuous Plankton Recorder: Towards a global perspective. J. Plankton. Res. *32*, 1619–1621
39. Quéguiner, B., and Tréguer, P. Studies on the phytoplankton in the Bay of Brest (Western Europe). (1984). Seasonal variations in composition biomass and production in relation to hydrological and chemical features (1981–1982). Bot. Mar. *27*, 449–459.
40. Del Amo, Y., Le Pape, O., Tréguer, P., Quéguiner, B., Menesguen, A., and Aminot, A. (1997). Impacts of high-nitrate freshwater inputs on macrotidal ecosystems. I. Seasonal evolution of nutrient limitation for the diatom-dominated phytoplankton of the Bay of Brest (France). Mar. Ecol. Prog. Ser. *161*, 213–224.
41. Boyce, D.G., Lewis M.R., and Worm, B. (2010). Global phytoplankton decline over the past century. Nature *466*, 591–596.
42. Burrows, M.T., Bates, A.E., Costello, M.J., Edwards, M., Edgar, G.J., Fox, C.J., Halpern, B.S., Hiddink, J.G., Plinsky, M.L., Batt, R.D., Molinos, J.G., Payne, B.L., Schoeman, D.S.,

888 Stuart-Smith, R.D., and Poloczanska, E.S. (2019). Ocean community warming responses
889 explained by thermal affinities and temperature gradients. Nat. Clim. Change *9*, 959–963.
890 43. Liu, D., Shen, X., Di, B., Shi, Y., Keesing, J., and Wang, Y. (2013). Palaeoecological
891 analysis of phytoplankton regime shifts in response to coastal eutrophication. Mar. Ecol.
892 Prog. Ser. *475*, 1–14
893 44. Ibrahim, A., Capo, E., Wessels, M., Martin, I., Meyer, D., Schleheck, D., and Epp, L.S.
894 (2020) Anthropogenic impact on the historical phytoplankton community of Lake
895 Constance reconstructed by multimarker analysis of sediment-core environmental DNA.
896 Mol. Ecol. https://doi.org/10.1111/mec.15696
897 45. Capo, E. Domaizon, I., Maier, D., Debroas, D., and Bigler, C. (2017). To what extent is the
898 DNA of microbial eukaryotes modified during burying into lake sediments? A repeat-coring
899 approach on annually laminated sediments. J. Paleolim. *58*, 479–495.
900 46. Cao, X., Xu, X., Bian, R., Wang, Y., Yu, H., Xu Y., Duan, G., Bi, L., Chen, P., Gao, S.,
901 Wang, J., Peng, J., and Qu, J. (2020). Sedimentary ancient DNA metabarcoding delineates
902 the contrastingly temporal change of lake cyanobacterial communities. Water Res. doi:
903 10.1016/j.watres.2020.116077.
904 47. Bálint, M., Pfenninger, M., Grossart, H.-P., Taberlet, P., Vellend, M., Leibold, M.A.,
905 Englund, G., and Bowler D. (2018). Environmental DNA time series in ecology. Trends
906 Ecol. Evol. *12*. 945–957.
907 48. Monchamp, M.-E., Enache, J., Turko, P., Pomati, F., Rîşnoveanu, G., and Spaak, P. (2017).
908 Sedimentary and egg-bank DNA from 3 European lakes reveal concurrent changes in the
909 composition and diversity of cyanobacterial and *Daphnia* communities. Hydrobiologia *88*,
910 155–172.

911 49. Pal, S., Gregory-Eaves, I., and Pick, F.R. (2015). Temporal trends in cyanobacteria revealed
912 through DNA and pigment analyses of temperate lake sediment cores. J. Paleolimnol. *54*,
913 87–101.
914 50. Pawlowski, J., Kelly-Qui, M., Altermatt, F., Apothéloz-Perret-Gentil, L., Beja, P., Boggero,
915 A., Borja, A., Bouchez, A., Cordier, T., Domaizon, I., Feio, M.J., Filipe, A.F., Fornaroli, R.,
916 Graf, W., Herder, J., van der Hoorn, B., Jones, I., Sagova-Mareckova, M., Moritz., C.,
917 Barquín, J., Piggott, J.J., Pinna, M., Rimet, F., Rinkevich, B., Sousa-Santos, C., Specchia,
918 V., Trobajo, R., Vasselon, V., Vitecek, S., Zimmerman, J., Weigand, A., Leese, F., and
919 Kahlert, M., (2018). The future of biotic indices in the ecogenomic era: Integrating (e)DNA
920 metabarcoding in biological assessment of aquatic ecosystems. Sci. Total Environ. *637–*
921 *638*, 1295–1310.
922 51. Coclet, C., Garnier, C., Delphy, F., Jamet, D., Durrieu, G., Le Poupon, C., Mayer, and M.,
923 Misson, B. (2018). Trace metal contamination as a toxic and structuring factor impacting
924 ultraphytoplankton communities in a multicontaminated Mediterranean coastal area. Prog.
925 Oceanogr. *163*, 196–213.
926 52. Jia, J., Gao, Y., Lu., Y., Shi, K., Li, Z., and Wang, S. (2020). Trace metal effects on gross
927 primary productivity and its associative environmental risk assessment in a subtropical lake,
928 China. Environ. Pollut. *259*, 113848.
929 53. Kleppel, G.S., and McLaughlin, J.J.A. (1980). PCB toxicity to phytoplankton: effects of
930 dose and density-dependent recovery responses. Bull. Environm. Contam. Toxicol. *24*, 696–
931 703.
932 54. Herzi, F., Jean, N., Hlaili, A.S., and Mounier, S. (2014). Three-dimensional (3-D)
933 fluorescence spectroscopy analysis of the fluorescent dissolved organic matter released by
934 the marine toxic dinoflagellate *Alexandrium catenella* exposed to metal stress by zinc or
935 lead. J. Phycol. *50*, 665–674

936 55. Bausch, A.R., Boatta, F., Morton, P.L., McKee, K.T., Anderson, R.F., Gomes, H.R., and
937 Goes, J.I. (2017). Elevated toxic effect of sediments on growth of the harmful dinoflagellate
938 *Cochlodinium polykrikoides* under high CO_2. Aquat. Microb. Ecol. *80*, 139–152.
939 56. Ragueneau, O., Chauvaud, L., Leynaert, A., Thouzeau, G., Paulet, Y.M., Bonnet., Lorrain
940 A, Grall, J., Corvaisier, R., Le Hir, M., Jean, F., and Clavier, J. (2002). Direct evidence of
941 a biologically active coastal silicate pump: Ecological implications. Limnol. Oceanog. *47*,
942 1849–1854.
943 57. Guillaud, J.-F., and Bouriel, L. (2007). Relation concentration-débit et évolution temporelle
944 du nitrate dans 25 rivières de la région Bretagne (France). Revue Des Sciences de L'eau,
945 *20*, 213.
946 58. Trommer, G., Leynaert, A., Klein, C., Naegelen, A., and Beker, B. (2013). Phytoplankton
947 phosphorus limitation in a North Atlantic coastal ecosystem not predicted by nutrient load.
948 J. Plank. Res. *35*, 1207–1219.
949 59. Reimer, P.J., Bard, E., Bayliss, A., Beck, J.W., Blackwell, P.G., Ramsey, C.B., Buck, C.E.,
950 Cheng, H., Edwards, R.L., Friedrich, M., Grootes, P.M., Guilderson, T.P., Haflidason, H.,
951 Hajdas, I., Hatté, H., Heaton, T.J., Hoffmann, D.L., Hogg, A.G., Hughen, K.A., Kaiser, K.
952 F., Kromer, B., Manning, S.W., Niu, M., Reimer, R.W., Richards, D.A., Scott,
953 E.M.,Southon, J.R., Staff, R.A., Turney, C.S.M. and van der Plicht, J. (2013). IntCal13 and
954 Marine13 radiocarbon age calibration curves 0–50,000 years cal BP. Radiocarbon *55*, 1869–
955 1887.
956 60. Gregoire, G., Le Roy, P., Ehrhold, A., Jouet, G., and Garlan, T. (2017). Control factors of
957 Holocene sedimentary infilling in a semi-closed tidal estuarine-like system: the bay of Brest
958 (France). Mar. Geol. *385*, 84–100.
959 61. Kim, J.H., Kim, J.H., Wang, P., Park, B.S., and Han, M.S. (2016). An improved quantitative
960 real-time PCR assay for the enumeration of *Heterosigma akashiwo* (Raphidophyceae) cysts

961 using a DNA debris removal method and a cyst-based standard curve. PLoS One *11*,
962 e0145712.
963 62. Gilbert, M.T. P., Bandelt, H.-J., Hofreiter, M., and Barnes, I. (2005). Assessing ancient
964 DNA studies. Trends Ecol Evol *20*, 541–544.
965 63. Martin, M. (2011). Cutadapt removes adapter sequences from high-throughput sequencing
966 reads. EMBnet J *17*, 10–12.
967 64. Callahan, B.J., McMurdie, P.J., Rosen, M.J., Han, A.W., Johnson, A.J.A., and Holmes, S.P.
968 (2016). DADA2: high-resolution sample inference from Illumina amplicon data. Nat.
969 Methods *13*, 581–583.
970 65. Guillou, L., Bachar, D., Audic, S., Bass, D., Berney, C., Bittner, L., Boutte, C., Burgaud,
971 G., de Vargas, C., Decelle, J., del Campo, J., Dolan, J.R., Dunthorn, M., Edvardsen, B.,
972 Holzmann, M., Kooistra, W.H.C.F., Lara, E., Le Bescot, N., Logares, R., Mahé, F.,
973 Massana, R., Montresor, M., Morard, R., Not, F., Pawlowski, J., Probert, I., Sauvadet, A.-
974 L., Siano, R., Stoeck, T., Vaulot, D., Zimmermann, P., and Christen, R. (2013). The protist
975 Ribosomal reference database (PR^2): a catalog of unicellular eukaryote small subunit rRNA
976 sequences with curated taxonomy. Nucleic Acids Res. *41*, D597–D604.
977 66. Okasenen, J., Kindt, R., Legendre, P., O'Hara, B., Simpson, G.L., Solymos, P., Henry, M.,
978 Stevens, H., and Wagner, H. (2008). The vegan Package. http://cran.r-project.org/,
979 http://vegan.r-forge.r-project.org.
980 67. McMurdie, P.J, and Holmes S (2013). phyloseq: An R package for reproducible interactive
981 analysis and graphics of microbiome census Data. Plos One *8*, e61217.
982 68. Horri, K., Alfonso, S., Cousin, X., Munschy, C., Loizeau, V., Aroua S., Bégout, M.-L., and
983 Ernande, B. (2018). Fish life-history traits are affected after chronic dietary exposure to an
984 environmentally realistic marine mixture of PCBs and PBDEs. Sci. Tot. Environ. *610–611*,
985 531–545

69. Breivik, K., Sweetman, A., Pacyna, J.M., and Jones, K.C. (2002). Towards a global historical emission inventory for selected PCB congeners — a mass balance approach: 2. Emissions. Sci. Tot. Environ. *290*, 199–224.

70. R Core Team R: A Language and Environment for Statistical Computing. R Foundation for Statistical Computing, Vienna. https://www.R-project.org (2018).

71. Wickham, H. (2009). Ggplot2. Elegant Graphics for data analysys (Springer International Publishing).

72. De'ath, G. (2002) Multivariate regression trees: a new technique: a new technique for modeling species - environment relationships. Ecology *83*, 1105–1117.

73. Borcard, D., Gillet, F., and Legendre, P. (2011) Numerical Ecology with R. (Springer, New York).

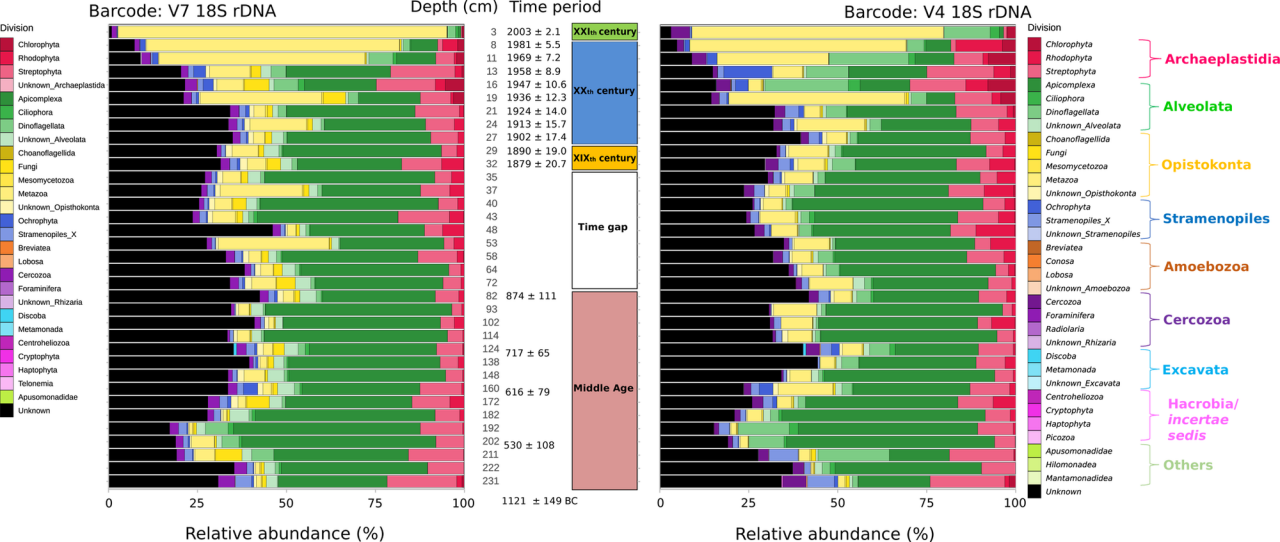
Barcode: V7 18S rDNA
Depth (cm)
Time period
Division
Chlorophyta
Rhodophyta
Streptophyta
Unknown_Archaeplastida
Apicomplexa
Ciliophora
Dinoflagellata
Unknown_Alveolata
Choanoflagellida
Fungi
Mesomycetozoa
Metazoa
Unknown_Opisthokonta
Ochrophyta
Stramenopiles_X
Breviatea
Lobosa
Cercozoa
Foraminifera
Unknown_Rhizaria
Discoba
Metamonada
Centroheliozoa
Cryptophyta
Haptophyta
Telonemia
Apusomonadidae
Unknown
3 2003 ± 2.1
8 1981 ± 5.5
11 1969 ± 7.2
13 1958 ± 8.9
16 1947 ± 10.6
19 1936 ± 12.3
21 1924 ± 14.0
24 1913 ± 15.7
27 1902 ± 17.4
29 1890 ± 19.0
32 1879 ± 20.7
35
37
40
43
48
53
58
64
72
82 874 ± 111
93
102
114
124 717 ± 65
138
148
160 616 ± 79
172
182
192
202 530 ± 108
211
222
231
1121 ± 149 BC
XXIm century
XXth century
XIXth century
Time gap
Middle Age
0
25
50
75
100
Relative abundance (%)
Barcode: V4 18S rDNA
Division
Chlorophyta
Rhodophyta
Streptophyta
Apicomplexa
Ciliophora
Dinoflagellata
Unknown_Alveolata
Choanoflagellida
Fungi
Mesomycetozoa
Metazoa
Unknown_Opisthokonta
Ochrophyta
Stramenopiles_X
Unknown_Stramenopiles
Breviatea
Conosa
Lobosa
Unknown_Amoebozoa
Cercozoa
Foraminifera
Radiolaria
Unknown_Rhizaria
Discoba
Metamonada
Unknown_Excavata
Centroheliozoa
Cryptophyta
Haptophyta
Picozoa
Apusomonadidae
Hilomonadea
Mantamonadidea
Unknown
Archaeplastidia
Alveolata
Opistokonta
Stramenopiles
Amoebozoa
Cercozoa
Excavata
Hacrobia/ incertae sedis
Others
0
25
50
75
100
Relative abundance (%)

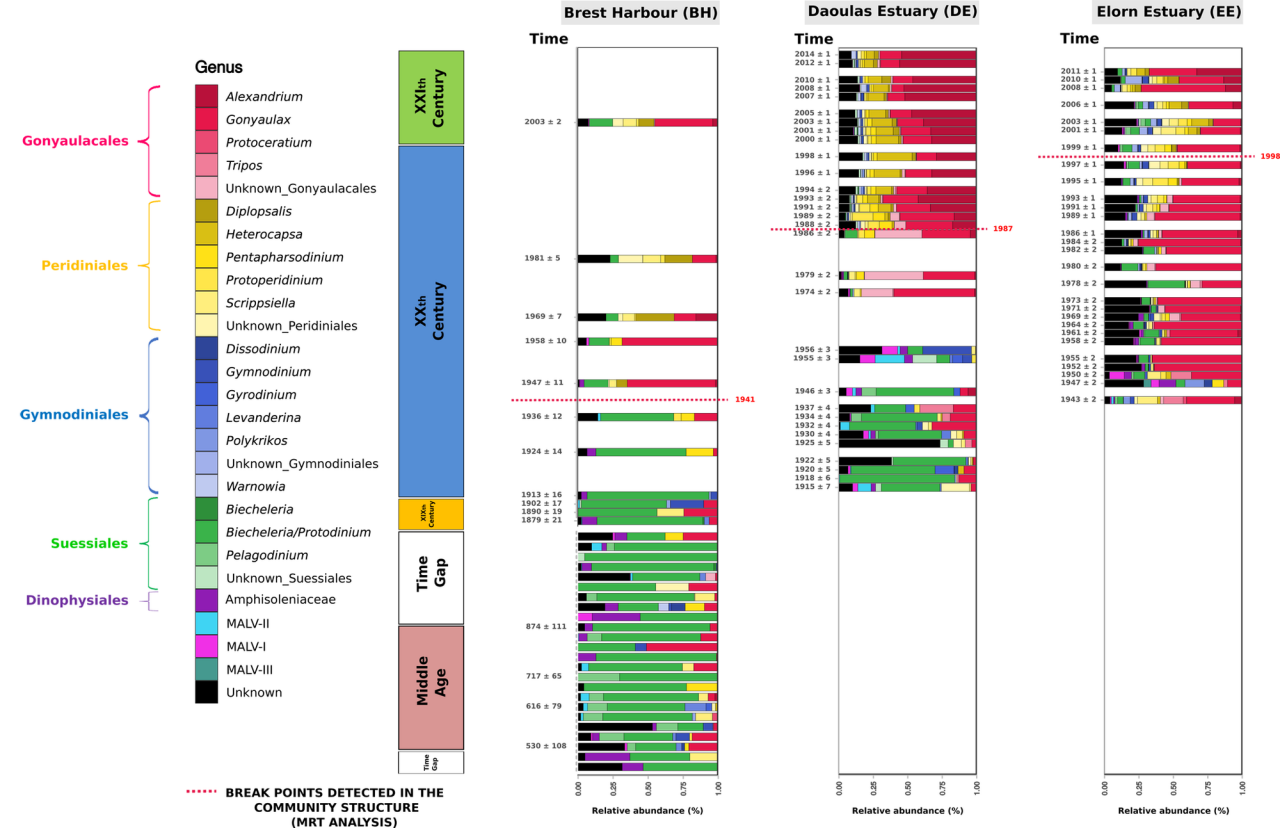
Brest Harbour (BH)
Daoulas Estuary (DE)
Elorn Estuary (EE)
Time
Genus
Gonyaulacales
Peridiniales
Gymnodiniales
Suessiales
Dinophysiales
Alexandrium
Gonyaulax
Protoceratium
Tripos
Unknown_Gonyaulacales
Diplopsalis
Heterocapsa
Pentapharsodinium
Protoperidinium
Scrippsiella
Unknown_Peridiniales
Dissodinium
Gymnodinium
Gyrodinium
Levanderina
Polykrikos
Unknown_Gymnodiniales
Warnowia
Biecheleria
Biecheleria/Protodinium
Pelagodinium
Unknown_Suessiales
Amphisoleniaceae
MALV-II
MALV-I
MALV-III
Unknown
XXIth Century
XXth Century
Time Gap
Middle Age
1941
1987
1998
BREAK POINTS DETECTED IN THE COMMUNITY STRUCTURE (MRT ANALYSIS)
Relative abundance (%)

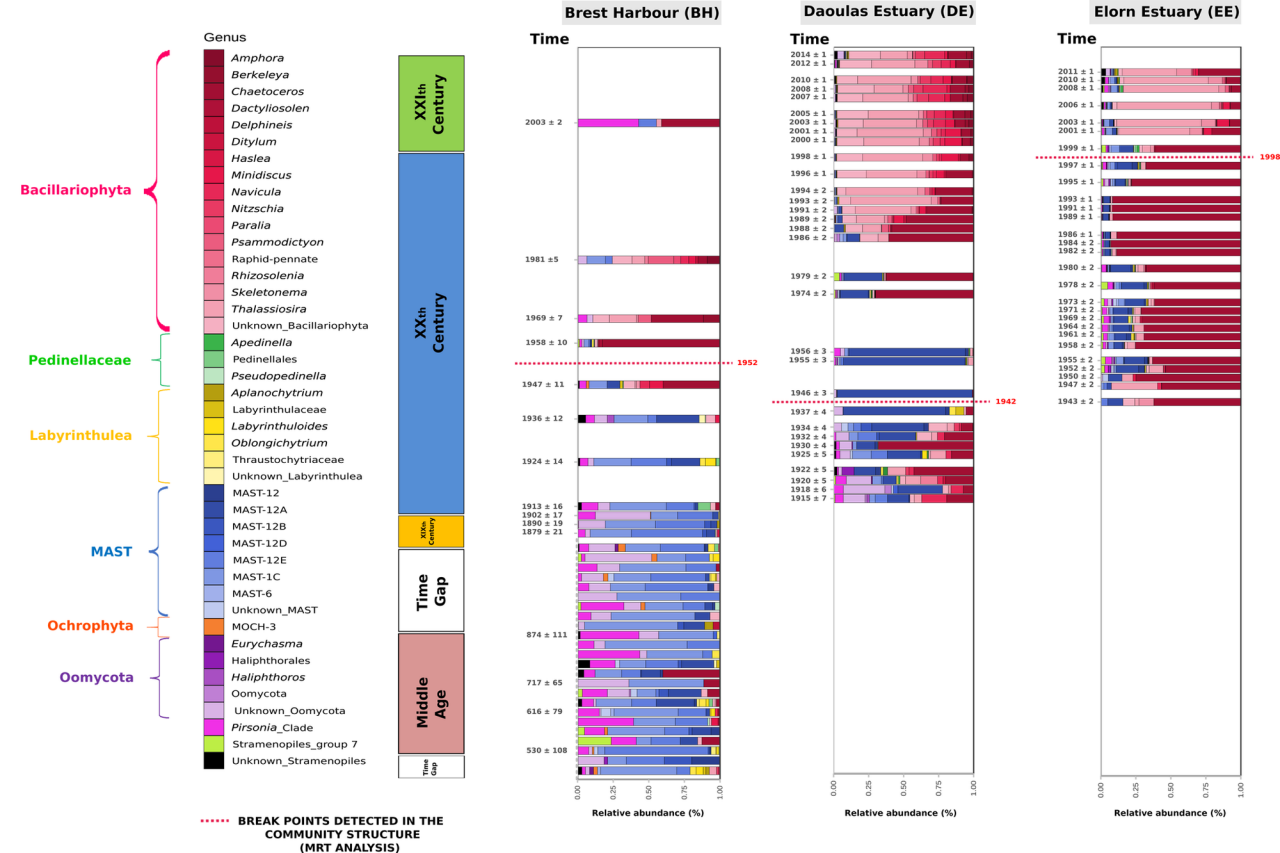
Genus
Amphora
Berkeleya
Chaetoceros
Dactyliosolen
Delphineis
Ditylum
Haslea
Minidiscus
Navicula
Nitzschia
Paralia
Psammodictyon
Raphid-pennate
Rhizosolenia
Skeletonema
Thalassiosira
Unknown_Bacillariophyta
Apedinella
Pedinellales
Pseudopedinella
Aplanochytrium
Labyrinthulaceae
Labyrinthuloides
Oblongichytrium
Thraustochytriaceae
Unknown_Labyrinthulea
MAST-12
MAST-12A
MAST-12B
MAST-12D
MAST-12E
MAST-1C
MAST-6
Unknown_MAST
MOCH-3
Eurychasma
Haliphthorales
Haliphthoros
Oomycota
Unknown_Oomycota
Pirsonia_Clade
Stramenopiles_group 7
Unknown_Stramenopiles
Bacillariophyta
Pedinellaceae
Labyrinthulea
MAST
Ochrophyta
Oomycota
XXIth Century
XXth Century
XIXth Century
Time Gap
Middle Age
Time Gap
Brest Harbour (BH)
Time
2003 ± 2
1981 ±5
1969 ± 7
1958 ± 10
1952
1947 ± 11
1936 ± 12
1924 ± 14
1913 ± 16
1902 ± 17
1890 ± 19
1879 ± 21
874 ± 111
717 ± 65
616 ± 79
530 ± 108
0.00
0.25
0.50
0.75
1.00
Relative abundance (%)
Daoulas Estuary (DE)
Time
2014 ± 1
2012 ± 1
2010 ± 1
2008 ± 1
2007 ± 1
2005 ± 1
2003 ± 1
2001 ± 1
2000 ± 1
1998 ± 1
1996 ± 1
1994 ± 2
1993 ± 2
1991 ± 2
1989 ± 2
1988 ± 2
1986 ± 2
1979 ± 2
1974 ± 2
1956 ± 3
1955 ± 3
1946 ± 3
1942
1937 ± 4
1934 ± 4
1932 ± 4
1930 ± 4
1925 ± 5
1922 ± 5
1920 ± 5
1918 ± 6
1915 ± 7
0.00
0.25
0.50
0.75
1.00
Relative abundance (%)
Elorn Estuary (EE)
Time
2011 ± 1
2010 ± 1
2008 ± 1
2006 ± 1
2003 ± 1
2001 ± 1
1999 ± 1
1998
1997 ± 1
1995 ± 1
1993 ± 1
1991 ± 1
1989 ± 1
1986 ± 1
1984 ± 2
1982 ± 2
1980 ± 2
1978 ± 2
1973 ± 2
1971 ± 2
1969 ± 2
1964 ± 2
1961 ± 2
1958 ± 2
1955 ± 2
1952 ± 2
1950 ± 2
1947 ± 2
1943 ± 2
0.00
0.25
0.50
0.75
1.00
Relative abundance (%)
BREAK POINTS DETECTED IN THE COMMUNITY STRUCTURE (MRT ANALYSIS)

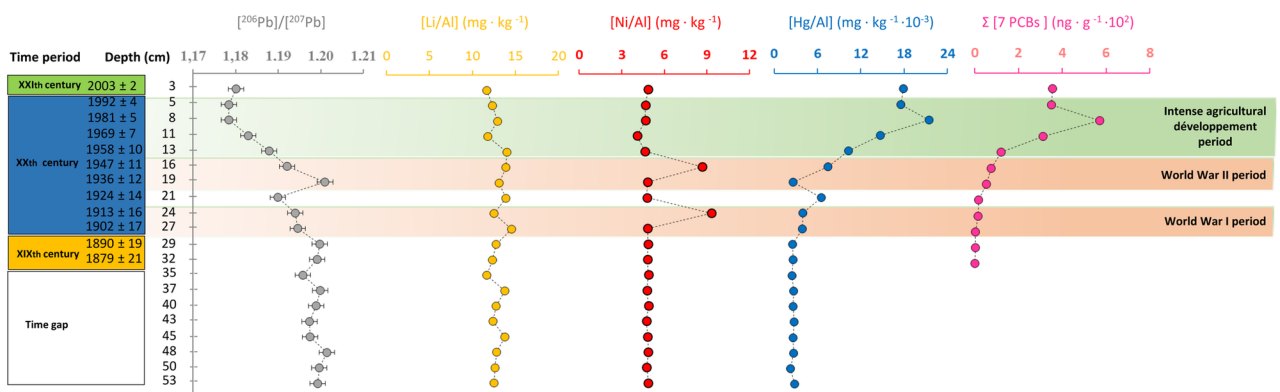
[206Pb]/[207Pb]
[Li/Al] (mg · kg -1)
[Ni/Al] (mg · kg -1)
[Hg/Al] (mg · kg -1 ·10-3)
Σ [7 PCBs] (ng · g -1 ·10²)
Time period
Depth (cm)
1,17 1,18 1,19 1,20 1,21
0 5 10 15 20
0 3 6 9 12
0 6 12 18 24
0 2 4 6 8
XXIth century 2003 ± 2
XXth century 1992 ± 4
1981 ± 5
1969 ± 7
1958 ± 10
1947 ± 11
1936 ± 12
1924 ± 14
1913 ± 16
1902 ± 17
XIXth century 1890 ± 19
1879 ± 21
Time gap
3
5
8
11
13
16
19
21
24
27
29
32
35
37
40
43
45
48
50
53
Intense agricultural développement period
World War II period
World War I period

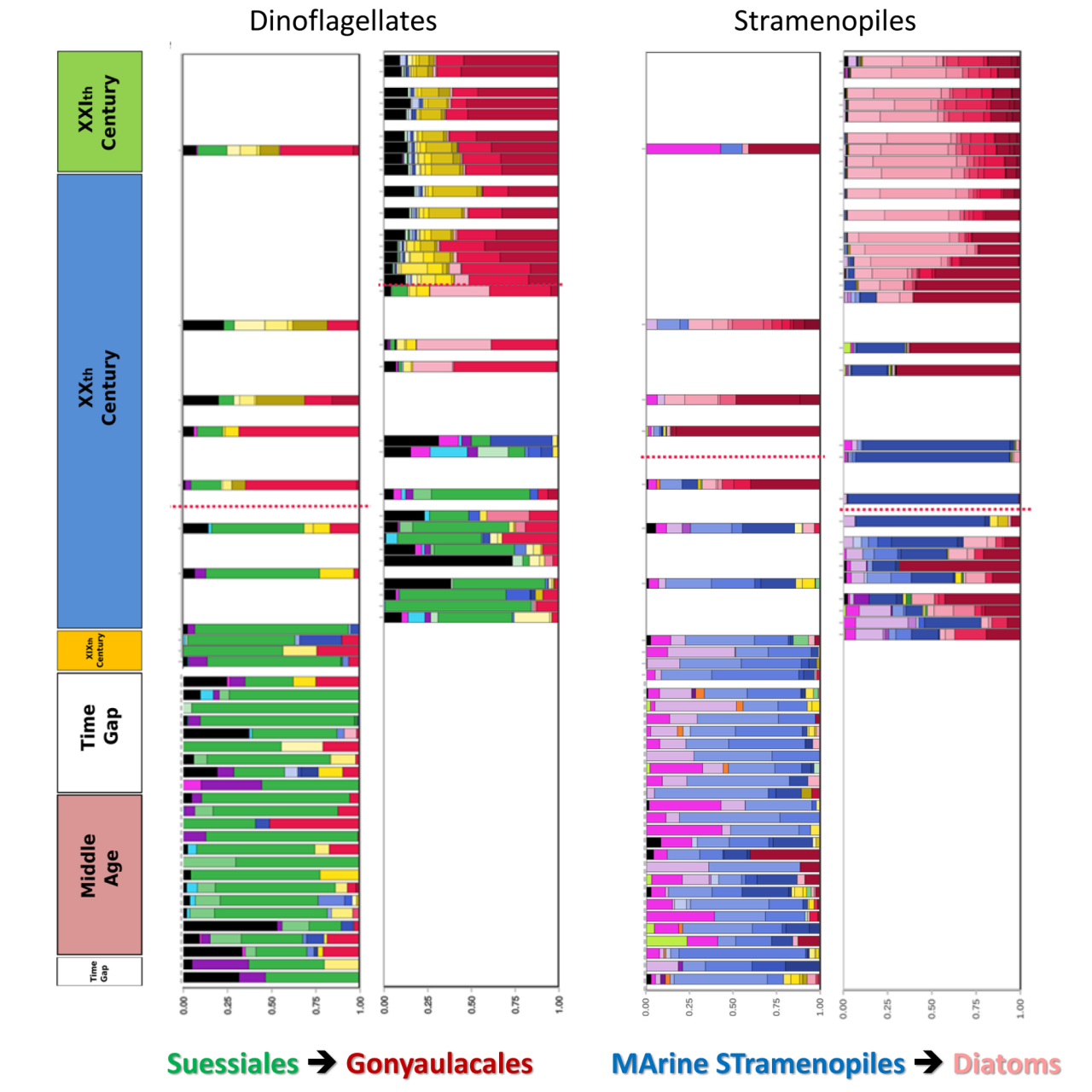
Dinoflagellates
Stramenopiles
XXIth Century
XXth Century
XIXth Century
Time Gap
Middle Age
Time Gap
0.00
0.25
0.50
0.75
1.00
Suessiales → Gonyaulacales
MArine STramenopiles → Diatoms